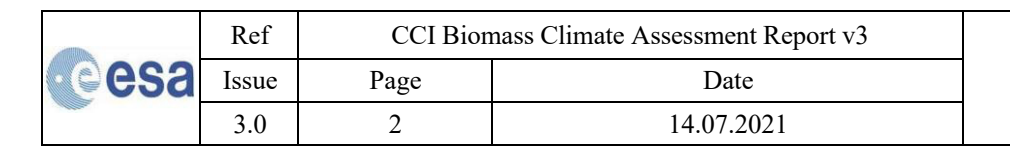
## CCI BIOMASS Phase IV

# CLIMATE ASSESSMENT REPORT YEAR 3 VERSION 1.0

DOCUMENT REF:	CCI_BIOMASSAGB_CAR_V3
DELIVERABLE REF:	D5.1_CAR
VERSION:	1.0
CREATION DATE:	2025-07-01
LAST MODIFIED	





#### Document Authorship

	NAME	FUNCTION	ORGANISATION	SIGNATUR E	DATE
Prepared	P. Ciais	WP5000 Lead	LSCE		
Prepared	Y. Xu	WP5000 researcher	LSCE		
Prepared	F. Ritter		LSCE		
Prepared	M. Santoro		Gamma		
Prepared	W. Li		U Tsinghua		
Prepared	R. Lucas	Project Manager	Aberystwyth University		
Verified	S. Quegan	Science Leader	Sheffield University		
Approved					

#### **Document Distribution**

Organisation	Name	Quantity
ESA	Frank Seifert	

#### **Document History**

VERSION	DATE	DESCRIPTION	APPROVED
0.1	2025-07-01	First draft version	
1.0	2025-07-01	Finalised version	

#### Document Change Record (from Year 1 to Year 2)

VERSION	DATE	DESCRIPTION	APPROVED

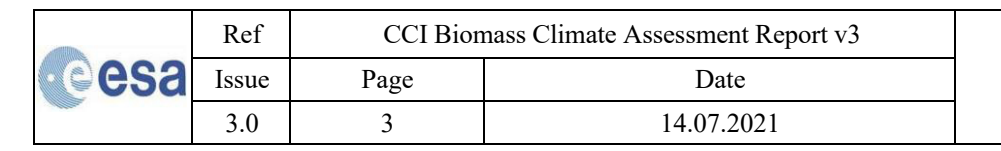
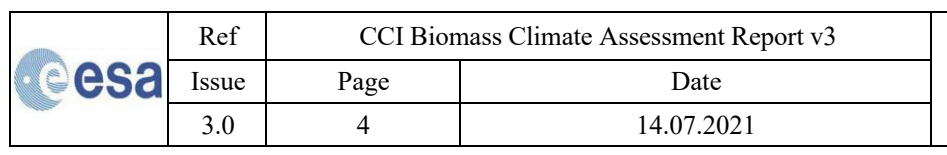




#### **TABLE OF CONTENTS**

LIS	T OF	FIGURES	4
LIS	T OF	TABLES	7
SYN	ивоі	S AND ACRONYMS	8
1	Sun	nmary	9
2	Ala	rming decline in the carbon sink of European forests driven by disturbances	10
2	2.1.2	Method  I model the forest regrowth	11 12
2	2	Forest biomass recovery	16
2	3	Carbon storage potential in a world without disturbance	18
2	.4	Inconsistencies in biomass change detection using remote sensing	20
2	5	Future carbon sink of Europe's forests	20
2	.6	Challenges and mitigation strategies	21
2	7	Conclusion	23
2	8	Reference	24
3.	Dist	turbance-recovery dynamics drive global forest biomass change	27
3	3.1.3 3.1.3 3.1.4	Method  Delineation of forest disturbances  Biomass dataset  Model the forest carbon gain and losses for the disturbed forest  Estimation of AGC changes for the undisturbed forest  Estimation of AGC fluxes and turnover times	28 31 32
3	.2	Global disturbed forest distribution and young forest age distribution	35
3	.3	Forest regrowth patterns across global regions	36
3	.4	Spatial and temporal dynamics of forest AGC change associated with disturba	
3	.5	Forest regrowth patterns across global regions	
3	6	Reference	





11

#### LIST OF FIGURES

Figure 2-1 Forest state in Europe during the historical period. (A) Above-ground biomass for the year 2019, averaged from two products: CCI-ESA (solid lines in the histograms) and PlanetScope (dashed lines), both biascorrected with NFI data at a sub-national scale. Histograms show the distributions within five biogeographical regions indicated in the miniature. (B) Trends in the mean percentage of forest cover loss at 18 km. The annual forest cover loss has been aggregated from 30 m to 18 km, divided by the forest area at 18 km. Then, a moving average (30-year window) has been computed to produce the mean percentage of forest cover loss (six values from 2000 to 2005). A linear trend has been computed at 18 km based on these six values (no trend corresponds to p > 0.05). Scatterplots display the annual percentage of forest cover loss due to all disturbances (natural and anthropogenic) in each biogeographical region. They were obtained by spatially aggregating the forest cover loss (at 30 m) across each biogeographical region, and then dividing by the total forest cover of the region. (C) Disturbance partitioning assessed from ground-based (1) and Landsat-based (2) data. The disturbance agents "bark beetles" and "others" have been merged with "storms" and "harvests" (respectively) due to Landsat's limited sensitivity. The ground-based partitioning was first established between harvests and natural disturbances (period 2001-2019, natural disturbances accounted for 16% of the mean annual harvest in Europe), then the natural disturbances was further partitioned following numbers given in (1) corresponding to the period 1950-2019 (D) Country reports to UNFCCC giving ground-based estimations from 2010 to 2021 of forest area (FA, Mha) and the forest sink (FS in MgC/haF), which is the sum of the net carbon stock change in the AGC, belowground-biomass, organic and mineral soils, deadwood, litter and harvested wood products. Four groups are separated based on the national forest sink trends: small decrease (in orange), large decrease (in red), and increase (in green) and no trend (in gray). The unit haf stands for hectares of forests.

Figure 2-5 **Forest growth in Europe.** (A) AGC recovery curves computed at 18 km based on a Chapman-Richard equation: AGCCRt = AGCpot(1-e-bt)c using two AGC datasets (CCI-ESA in blue, and PlanetScope in red) harmonized with NFI data on a sub-national scale. See supplementary Fig. 2-6 for a map of coefficients b, c, and AGCpot. The representative growth curve (thick line) is obtained with the median of all valid curves associated with a r2 > 0.5 in a specific biogeographical region. Points represent the median of the AGC after a stand-replacing disturbance (limited to 5-30 years based on the Landsat range) or the median of the

© Aberystwyth University and GAMMA Remote Sensing, 2018

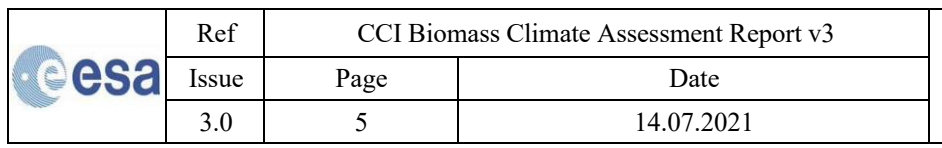


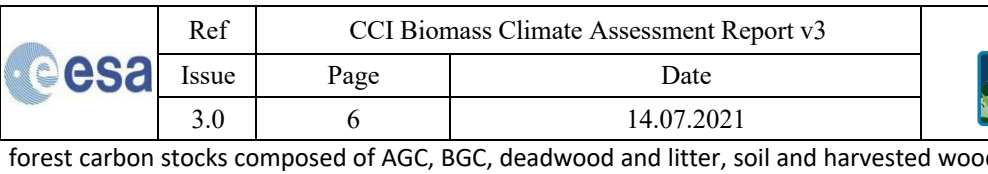


Figure 2-6 Chapman-Richards coefficients from the recovery curves. The Chapman-Richards growth function is decribed as  $AGC(t)=AGC_{pot}$  (1-e(-b\*t))^c. **A**, Growth coefficients obtained from the parameterization of the DDCM at a country scale for the PlanetScope AGC map. **B**, Growth coefficients obtained from the parameterization of the DDCM at a country scale for the CCI-ESA AGC maps. **C**, growth coefficients obtained from the parameterization of the DDCM at a regional scale for the PlanetScope AGC map. **D**, growth coefficients obtained from the parameterization of the DDCM at a regional scale for the CCI-ESA AGC maps. Missing values in these maps will be filled with spatial interpolations before simulating the AGC from 2010 to 2020.

Figure 2-7. Changes in forest growth and disturbances, DDCM procedure, and remote sensing inconsistencies in biomass change. (A) Comparison across Europe of the mean AGC (CCI-ESA, bias-corrected with NFI data on a sub-national scale) of forests from 5 to 30 years old (Landsat range) between the periods 2015-2017 and 2019-2021. For each year (2015,2016,2017,2019,2020,2021), the mean AGC of forests (for a given age class) has been aggregated from 30 m to 18 km. One point in panel A corresponds to the mean value of all 18 km pixels across Europe for the given period (2015-2017 for the X axis and 2019-2021 for the Y axis) and a given age class. (B) The volume of wood loss is shown in blue (1) and the percentage of forest cover loss is shown in red (2) due to natural disturbances in the EU-27 from 2010 to 2019. (C) Roundwood removals are shown in blue (3) and the percentage of forest cover loss is shown in red (2) due to harvest or salvage logging in the EU-27 from 2010 to 2020. The percentage of forest cover loss has been aggregated from the same sub-sample of Europe described in panel B. (D) Example of AGC simulations from the data-driven carbon model (DDCM) for a forested pixel at 18 km, from two AGC datasets (the year 2019 for PlanetScope and mean of 2017-2021 for CCI-ESA) and one parameterization (bootstrap conducted on each country). See Fig. 2-3 for more details. The simulated AGC is the mean of 50 replicates. For each replicate, the period of growth is equal to the return interval, which is the average time between two mean disturbances aggregated at 18 km across 30-year windows (typically between 1 and 5 years). Each replicate has a different starting time of the first disturbance. The mean percentage of AGC loss at 18 km is scaled from the mean percentage of forest cover loss with a bootstrap analysis that minimizes the difference between simulated and observed (UNFCCC) annual changes in AGC from 2010 to 2021. (E) Annual AGC changes from CCI-ESA maps (2015 to 2021), UNFCCC reports, and DDCM simulations from 2010 to 2021 (PlanetScope has only one year of data and changes cannot be assessed). Annual AGC changes for CCI-ESA (2016-2021) have been aggregated across each biogeographical region, regardless of the quality flag of the CCI-ESA product or possible 0 values emerging 

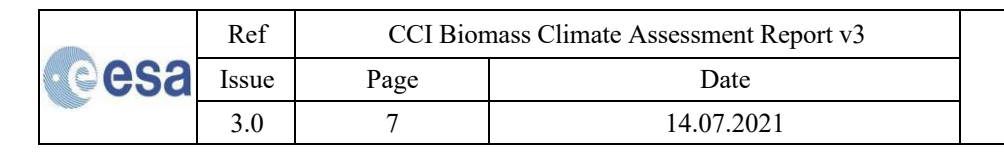
Figure 2-8 **Spatial and temporal changes in the carbon sink of European forests.** (**A**) Forest sinks for the five biogeographical regions and the EU-27 are based on two forest management scenarios: business as usual and a 26% decrease in harvest in addition to the 3 billion trees planted by 2030 (their total forest sink is pink). The forest sink is the sum of five components: net carbon stock change in the AGC, below-ground biomass (BGC), deadwood and litter, soils and harvested wood products. The EU-27 forest sink target has been estimated at 392 MtCO<sub>2</sub>eq, the average for the years 2016-2018. The black-shaded area represents the total variability obtained from using PlanetScope or CCI-ESA maps with the parameterization conducted per country or biogeographical region. (**B**) Map of the difference between 2030 and 2010 of the AGC simulated by the DDCM. Forests losing AGC from 2010 to 2030 are in yellow. (**C**) Map of the difference between 2030 and 2010 of the

orests losing AGC from 2010 to 2030 are in yellow. (**C**) Map of the difference between 2030 and 2010 of the





	3.0	6	14.07.2021	CCI		
forest carbon	stocks co	omposed of AGC, E	BGC, deadwood and litter, soil and harvested	d wood products (values		
have been divided by 2 to match the legend). Forests losing carbon (acting as a source) from 2010 to 2030 are						
-	-		sistencies between CCI-ESA and PlanetScop			
product predi	icts a cark	oon source and the	e other a carbon sink)	21		
Figure 3-1 Co	nceptual	diagram		28		
disturbed dur showing the ageing forest groups (0–10	ing 1985- proportic s that rer , 11–20,	2020 within each a on of young forest mained undisturbe 21–30, and 31–40	d forests and forest age structure in 2020. a 1° grid cell. b) Forest age composition in 202 ts that regenerated following disturbances ed over the same period. Young forests are years) based on the time since the last dispoundaries correspond to those shown in Fig	0, with each donut chart during 1985–2020 and classified into four age sturbance, derived from		
as a function years after reg (c) Regional n AGC growth exp(-bt))°)+d	of forest growth w nap used curves at based on	age for each study ith estimates from in the analysis. Ea 1° grid cell were the time since the	AGC) accumulation changes with time. (a) Fy region. (b) Comparison of AGC accumulation naturally regenerating forests reported by Coch color-coded region corresponds to those fitted using the Richards-Chapman functional elast disturbance (t) derived from the region ethods).	con rates over first 0-100 Cook-Patton et al. $(2020)^2$ . The used in panels a and b. For $(AGC = AGC_{max} \times (1 - nal disturbance histories)$		
2020. (a) Spat of AGC change Black lines ind availability va States (1990– (i.e., Other Bo	tial patter e by study dicate the ries by re -2015), th oreal and	rns of gross AGC ga y region. Bars show e annual net AGC gion based on the e Tropics (1990–20 Other regions), a g	cs of forest AGC change associated with distants, gross AGC losses, and net AGC changes annual carbon losses and gains due to fire a balance, calculated as the sum of all carbon coverage of regional disturbance datasets: 020), and Australia (1988–2020). In regions clobal burned area dataset was used 21. Note the due to limited Landsat availability	s. (b) Temporal dynamics and non-fire disturbances. In flux components. Data for example, the United lacking regional datasets at that fire data has an ~8-		
of AGC fluxes distribution of disturbances	s, calculat of AGC to during 19	red as the ratio of urnover time, def 085–2020. (b) Regi	gross AGC losses to total AGC stock at each fined as the ratio of total AGC stock to onal averages of AGC turnover rate and AGC stock (d), corresponding to the maps in a age.	ch 1° grid cell. (c) Spatial gross AGC losses from C turnover (PgC yr <sup>-1</sup> ), (d)		





#### LIST OF TABLES

Table 3-1 Disturbance datasets used in the analysis	29
Table 3-2 Forest extent data sources used in the analysis.	Error! Bookmark not defined.

	Ref	CCI Biomass Climate Assessment Report v3	
esa	Issue	Page	Date
	3.0	8	14.07.2021



#### SYMBOLS AND ACRONYMS

AGB Aboveground Biomass
AGC Aboveground Carbon
BGB Belowground Biomass
CAR Climate Assessment Report
CCI Climate Change Initiative
CLCD China land cover dataset
DDCM Data-Driven Carbon Model

EFDA European Forest Disturbance Atlas

DWL Deadwood and Litter
ESA European Space Agency

GABAM Global Annual Burned Area Map

GFW Global Forest Watch

HWP Harvested Wood Products

LC Land Cover

LUC Land Use Change

LCCMS Landscape Change monitoring System

TMF Tropical Moist Forest
RMSE Root Mean Square Error

	Ref	CCI Biomass Climate Assessment Report v3		
esa	Issue	Page	Date	
	3.0	9	14.07.2021	



#### 1 Summary

In the previous Climate Assessment Report (CAR) report from Phase I, we addressed the use of the European Space Agency (ESA) Climate Change Initiative (CCI) BIOMASS data on the Above Ground Biomass (AGB; Mg ha<sup>-1</sup>) of woody vegetation for evaluation of TRENDYV8 DGVMs, the inference of tropical land carbon cycle parameters by combining CCI BIOMASS AGB estimates, L-band Volumetric Optical Depth (LVOD) from Soil Moisture and Ocean Salinity (SMOS), Leaf Area Index (LAI) data, and the change of tropical AGB inferred from LVOD calibrated to AGB, with a focus on the recovery of AGB from the most recent El Niño.

In the Phase II CAR report, we applied CCI BIOMASS AGB data to infer forest biomass changes in three regional studies 1) the forest biomass loss caused by plantation area expansion in Southeast Asia, 2) the deficit and loss of AGB across forest edges in Africa, 3) the net carbon balance of boreal forests, with a focus on fire disturbances and post-fire AGB recovery.

In this Phase III CAR report, we applied CCI BIOMASS AGB data to infer the forest biomass losses and gains associated with fire, degradation, deforestation, and regrowth within tropical forests during 1990-2020. In this case study, we provided spatially explicit, long-term analysis of the carbon balance dynamics within disturbed tropical humid and dry forests, offering critical insights for accurate resource assessment, land management, and the formulation and monitoring of land use emission reduction policies.

In the initial version of the CAR from CCI BIOMASS Phase IV, we applied CCI BIOMASS AGB data to two studies aimed at quantifying carbon changes in forest ecosystems—one focusing on European forests and the other on global disturbed forests. For Europe, we modeled the EU-27 forest carbon sink from 2010–2030 using UNFCCC carbon data, disturbance maps and available AGB modeling. We found that, without intervention, the EU forest carbon sink will decline by 44% by 2030—falling 29% short of climate targets. The decline is primarily driven by increased disturbances and harvests, and the study concludes that reducing harvest levels by 26% is critical to reversing the trend. This study is currently under review and the full preprint is available at https://www.researchsquare.com/article/rs-3671432/v1. In the second study, we integrated CCI BIOMASS AGB data with the disturbance history (1985-2020) and regionally calibrated above-ground carbon (AGC; Mg ha<sup>-1</sup>) regrowth curves at 1° spatial resolution. Our analysis shows that forests disturbed since 1985 account for 30% of global forest area. These disturbed forests resulted in a net global AGC loss of -8.5 PgC, comprising -27.3 PgC from disturbance-related losses and +18.9 PgC from regrowth. Notably, 83% of the carbon losses occurred in tropical regions. AGC turnover rates varied globally, with the highest observed in Australia (1.17%) and the lowest in boreal regions such as Russia and Alaska (0.09%).

	Ref	CCI Biomass Climate Assessment Report v3	
esa	Issue	Page	Date
	3.0	10	14.07.2021



## 2 Alarming decline in the carbon sink of European forests driven by disturbances

European forests have gradually recovered from major timber exploitation during and following the two World Wars <sup>1</sup>. Today, they cover 33% of the continent and hold 12.1 PgC of aboveground biomass carbon (AGC, Fig. 2-1A), based on a recent dataset established from National Forest Inventories (NFIs) at sub-national scale for 2020 <sup>2</sup>. Forests constitute the main carbon sink of the European Union (EU-27), which has implemented a revised regulation aiming to achieve an annual carbon sink of 310 MtCO<sub>2</sub>eq in the land use sector by 2030 <sup>3</sup>. In this study, we define the forest carbon sink as the sum of five components: the net carbon stock change in AGC, below-ground biomass, soils (organic and mineral), deadwood and litter, and harvested wood products.

Despite their importance for carbon sequestration, Europe's forests are facing increasing pressure from timber harvest <sup>4,5</sup>, as well as from natural disturbances such as wildfires, storms, bark beetle outbreaks <sup>6</sup>, and drought and heatwave events <sup>7</sup>. Timber harvest is the most significant disturbance in Europe, accounting for 83-86% of all the forest area losses from 2001 to 2019, followed by storms (6-7%), fires (3-5%) and bark-beetles (less than 3%) based on the data from two independent studies <sup>6,8</sup>. The increasing rate of forest disturbances was already predicted in the 1990s <sup>9</sup> and has been confirmed by recent *in situ* <sup>6</sup> and satellite <sup>10</sup> observations. Over the past three decades, the mortality of forest trees has almost doubled in Europe <sup>11</sup>, raising concerns about the future resilience of forests to disturbances <sup>12</sup> and their capacity to maintain their role as major carbon sinks <sup>13-15</sup>. Annual summaries of country reports under the UNFCCC indicate that the carbon sink of 69% of European forests has declined from 2010 to 2021, despite the forest area of Europe increasing by 1.6% (Fig. 2-1D).

NFIs routinely monitor forest wood stocks through regular measurements of numerous field plots with statistical sampling schemes specific to each country <sup>16</sup>. However, inventories typically have a revisit cycle of five years, which complicates the tracking of changes in forest growth or stocks, and individual plot observations are not easily accessible to the scientific community due to economic interests and legislative issues (e.g., 47% of forests are privately owned <sup>4</sup>). Spaceborne remote sensing offers an attractive data source for obtaining spatially explicit estimates of forest carbon stocks. We used two state-of-the-art annual AGB maps: one from CCI-ESA v5 <sup>17</sup> (100 m resolution, 2015 to 2021) and another from PlanetScope imagery v0.1 <sup>18</sup> (30 m resolution aggregated from 3 m nanosatellite images, available for 2019). The AGB density is converted to AGC density using a scaling factor of 0.5 <sup>19</sup>. The two map products are independent, allowing for the assessment of uncertainties, and have been bias-corrected to align with the forest cover and AGC levels reported by NFIs at a sub-national scale <sup>2</sup>.

	Ref	CCI Biomass Climate Assessment Report v3	
esa	Issue	Page	Date
	3.0	11	14.07.2021



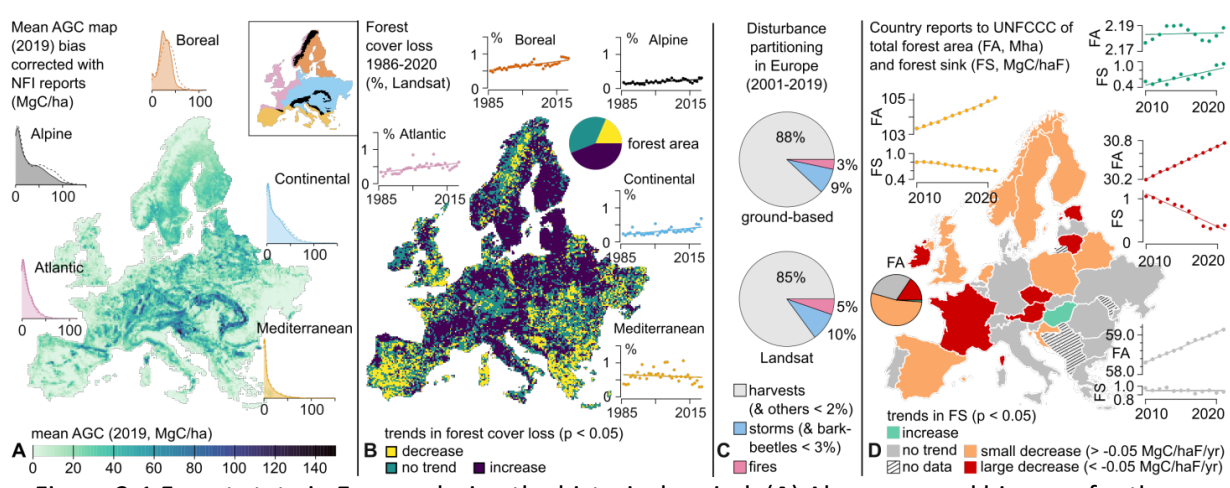
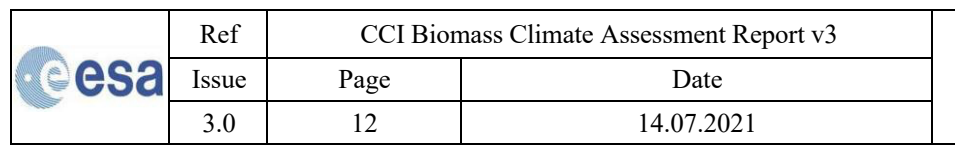


Figure 2-1 Forest state in Europe during the historical period. (A) Above-ground biomass for the year 2019, averaged from two products: CCI-ESA (solid lines in the histograms) and PlanetScope (dashed lines), both bias-corrected with NFI data at a sub-national scale. Histograms show the distributions within five biogeographical regions indicated in the miniature. (B) Trends in the mean percentage of forest cover loss at 18 km. The annual forest cover loss has been aggregated from 30 m to 18 km, divided by the forest area at 18 km. Then, a moving average (30-year window) has been computed to produce the mean percentage of forest cover loss (six values from 2000 to 2005). A linear trend has been computed at 18 km based on these six values (no trend corresponds to p > 0.05). Scatterplots display the annual percentage of forest cover loss due to all disturbances (natural and anthropogenic) in each biogeographical region. They were obtained by spatially aggregating the forest cover loss (at 30 m) across each biogeographical region, and then dividing by the total forest cover of the region. (C) Disturbance partitioning assessed from ground-based <sup>6</sup> and Landsat-based <sup>8</sup> data. The disturbance agents "bark beetles" and "others" have been merged with "storms" and "harvests" (respectively) due to Landsat's limited sensitivity. The ground-based partitioning was first established between harvests and natural disturbances (period 2001-2019, natural disturbances accounted for 16% of the mean annual harvest in Europe), then natural disturbances was further partitioned following numbers given in <sup>6</sup> corresponding to the period 1950-2019 (D) Country reports to UNFCCC giving groundbased estimates from 2010 to 2021 of forest area (FA, Mha) and the forest sink (FS in MgC/haF), which is the sum of the net carbon stock change in the AGC, belowground biomass, organic and mineral soils, deadwood, litter and harvested wood products. Four groups are separated based on the national forest sink trends: small decrease (in orange), large decrease (in red), and increase (in green) and no trend (in gray). The unit haF stands for hectares of forests.

#### 2.1 Method

#### 2.1.1 Model the forest regrowth

To assess current and predict future AGC changes, we leveraged a recent European disturbance map based on 30 m resolution Landsat data from 1986 to 2020 <sup>10</sup>. This map allowed us to estimate trends in AGC loss due to disturbances by spatially and temporally aggregating forest cover loss data from 30 m to 18 km. We also used two AGB maps (converted to AGC using a factor of 0.5 <sup>19</sup>), one CCI-ESA maps <sup>17</sup> (2015 to 2021, version 5, at 100 m resolution) and the 2019 PlanetScope-based AGC map <sup>18</sup> (30 m, version 0.1). All AGC maps have been bias-corrected to match the AGC reported at the sub-national scale in the harmonized NFI dataset for the year 2020 <sup>2</sup>. The correction for each European departmental unit is a multiplicative factor





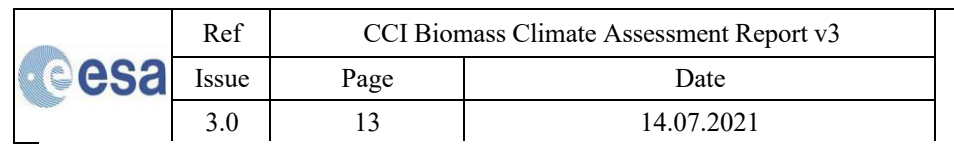
corresponding to the ratio between the AGC reported by NFIs and the mean raw AGC of 2020 for CCI-ESA or 2019 for PlanetScope. The median correction across all units (288) is  $1.30 \pm 0.27$  ( $\pm$  1 Mean Absolute Deviation) for CCI-ESA, and  $1.06 \pm 0.24$  ( $\pm$  1 MAD) for PlanetScope.

Then, we estimated AGC gains from forest regrowth following disturbances <sup>20</sup> using a space-fortime methodology following the approach originally developed for tropical forests <sup>21</sup>. We extended their approach and derived spatially explicit local recovery curves at 18 km across all Europe from two AGB maps (CCI-ESA Biomass and PlanetScope) instead of continental-average curves used in their work. The year of the disturbance is first subtracted from the year of the AGC map to obtain post-disturbance years. The AGC maps are then normalized by dividing them with  $AGC_{pot}$  defined here as  $AGC_{pot} = \alpha AGC_{75\%}$ , with  $AGC_{75\%}$  the 75% percentile of the AGC of all 30 m forests undisturbed since 1986 inside an 18 km pixel, and  $\alpha$  a correction factor calculated on the scale of a country or biogeographical region. For each AGC dataset (average of AGC maps from 2017-2021 for CCI-ESA, or PlanetScope map of 2019), values of  $(\alpha)$  have been estimated on a country-level or a biogeographical region-level using a bootstrap analysis that minimizes the RMSE between DDCM simulations and observations of ΔAGC from UNFCCC reports across the recent historical period (2010-2021). Then these ( $\alpha$ ) correction maps have been smoothed at 100 km to reduce the discrepancies at the border between two countries or two biogeographical regions. For each normalized AGC map (2015-2021 for CCI-ESA and 2019 for PlanetScope) and each 18 km pixel, five mean AGCs are calculated within five-time windows ([5-10 years], [10-15 years],..,[25-30 years]). For each time window, the average of the seven products of CCI-ESA (2015-2021) is computed to reduce uncertainties. A Chapman-Richard growth curve  $(AGC_{CR}(t) = AGC_{not}(1 - e^{-bt})^c)$  is fitted through the five values to estimate the b and c coefficients. Growth curves with non-physical inputs are discarded (AGC[5-10 years] > AGC[25-30 years]), and outliers in b and c populations across Europe are removed using the Logbox method. Growth curves associated with  $r^2 < 0.5$  are finally discarded. The time  $t_{\rm 90}$ required to recover 90% of the  $AGC_{pot}$  after a stand-replacing disturbance corresponds to  $AGC_{CR}(t_{90})=0.9AGC_{pot}$  which leads to  $t_{90}=-\frac{1}{h}log(1-0.9^{\frac{1}{c}})$ . The median  $t_{90}$  has been calculated from all 18 km pixels with valid growth curves. These curves have been validated with an independent in situ dataset on forest age and AGC 22.

#### 2.1.2 DDCM model overview

The data-driven carbon model (DDCM Version 1.1, Fig. 2-2 and Fig. 2-3) simulates annual AGC stocks from 2010 to 2030 at 18 km resolution. The net carbon stock change in AGC for a year y is computed as  $\Delta AGC(y) = AGC(y) - AGC(y-1)$ . According to UNFCCC reports, the carbon sink of forests across all five European biogeographical regions (miniature in Fig. 1A) is primarily driven by the net carbon stock change in AGC rather than in soils, deadwood, and harvested wood products. The net carbon stock changes in belowground biomass ( $\Delta BGC$ ), soils ( $\Delta S$ ), harvested wood products ( $\Delta HWP$ ), and deadwood (including litter,  $\Delta DWL$ ) are therefore estimated based on  $\Delta AGC$  with linear relationships derived from UNFCCC data in five different biogeographical regions (Fig. 2-4). This gives access to the annual forest sink at 18 km, defined as  $FS(y) = \Delta AGC(y) + \Delta BGC(y) + \Delta S(y) + \Delta HWP(y) + \Delta DWL(y)$ . Remote-sensing and ground-based data have been integrated into our study to reconcile differences that have sparked debate in these last years (see Matters Arising in Nature  $^{23}$ ).

The AGC(y) is computed from the imbalance between AGC gain due to forest growth and AGC loss due to disturbances. The annual percentage of AGC loss (s(y)) is modeled at 18 km resolution based on a linear relationship to capture long-term (30 years) trends in disturbance





rates (Fig. 2-1B). This linear relationship is obtained by applying a scaling factor  $\alpha$  (constant over a country or a biogeographical region) to forest cover loss data aggregated spatially and temporally from a Landsat-based disturbance map. AGC gains are modeled using an analytical growth curve at 18 km resolution (Fig. 2-1A) (Section 2.1.1). The growth curve is constrained by an upper limit, referred to as potential AGC ( $AGC_{pot}$ ), which is obtained by applying a scaling factor  $\beta$  (constant over a country or a biogeographical region) to AGC values of forests undisturbed since 1986. Then the two coefficients of the forest growth curve (b,c, see details in Section 2.1.1) are retrieved at 18 km knowing the age (obtained from the disturbance map, from 5 to 30 years old) and the AGC (obtained from the remote-sensing maps CCI-ESA or PlanetScope) of thousands of 30 m forested pixels inside each 18 km pixel. The two upscaling factors  $\alpha$  and  $\beta$  are parameterized at the scale of a country (or a biogeographical region) so that DDCM simulations match the UNFCCC observations (2010-2021, see Fig. 2-7E).

In particular, Version 1.1 of the DDCM (i) matches the forest cover and the AGC of European countries based on NFI data for the year 2020, (ii) does not simulate land-use change (the forest cover is constant), (iii) does not account for changes in the growth curves (for example  $CO_2$  fertilization effects are ignored), (iv) captures long-term trends (30-year periods) at 18 km in natural disturbances and harvests (Fig. 2-1B), and finally (v) ignores the AGC changes according to the maps from CCI-ESA (2015-2021, these are contaminated with artefacts, see Fig. 2-7E). A single year of AGC data (2019 for PlanetScope and mean of 2017-2021 for CCI-ESA) is used to run the DDCM from 2010 to 2030.

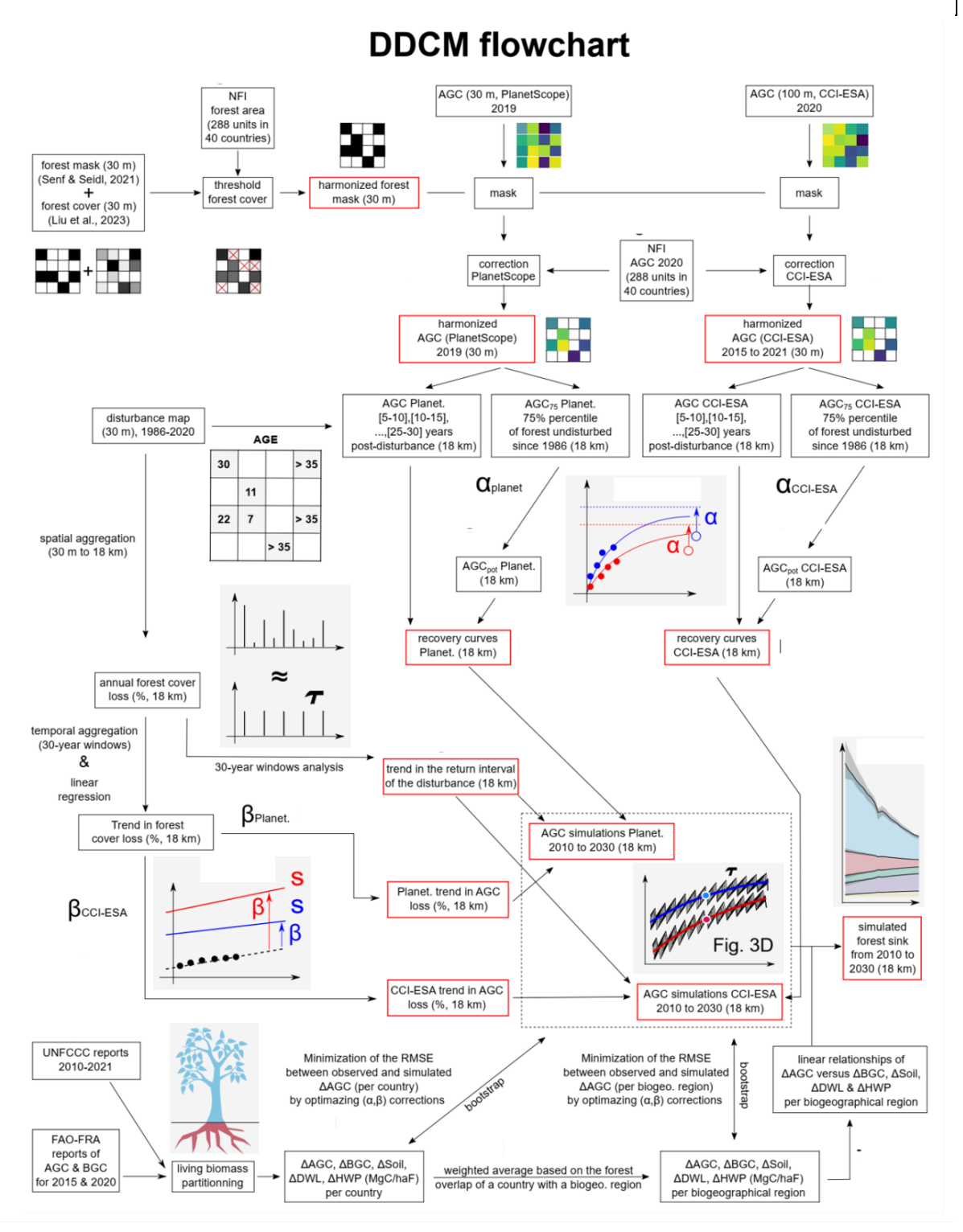


Figure 2-2 Flowchart of the DDCM procedure. This flowchart explains the DDCM procedure from raw data to forest sink estimates. The variable s refers to the percentage of AGC loss, and  $\tau$  to the return interval of the disturbances (for a 30-year window), both defined at 18 km. The correction factors  $(\alpha, \beta)$  are defined at a country or a biogeographical region scale.

	Ref	CCI Biomass Climate Assessment Report v3		
esa	Issue	Page	Date	
	3.0	15	14.07.2021	1



#### Example of the DDCM procedure for a 18 km forested pixel

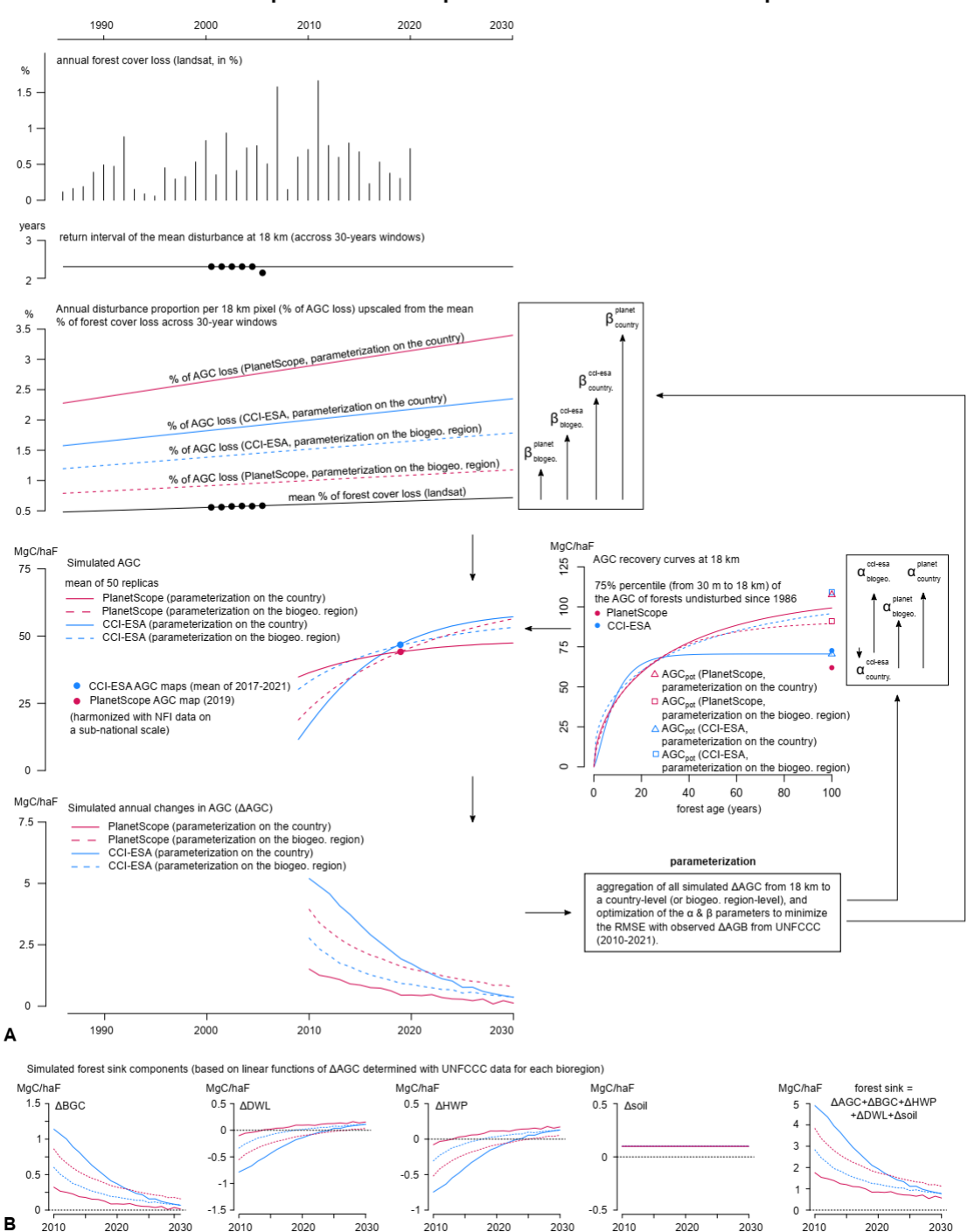


Figure 2-3 Detailed example of the DDCM procedure for a given forested pixel at 18 km. Use of the flowchart presented in Fig. 2-2 on an 18 km forested pixel. The parametrization is a bootstrap conducted on the scale of a country or a biogeographical region to adjust the correction factors  $(\alpha,\beta)$  so that the difference between simulated and observed (UNFCCC) annual changes in AGC is minimized across the historical period (2010-2021). Each forest sink component ( $\Delta$ HWP,  $\Delta$ Soil,  $\Delta$ BGC and  $\Delta$ DWL in panel B) is computed based on  $\Delta$ AGC using linear relationships.

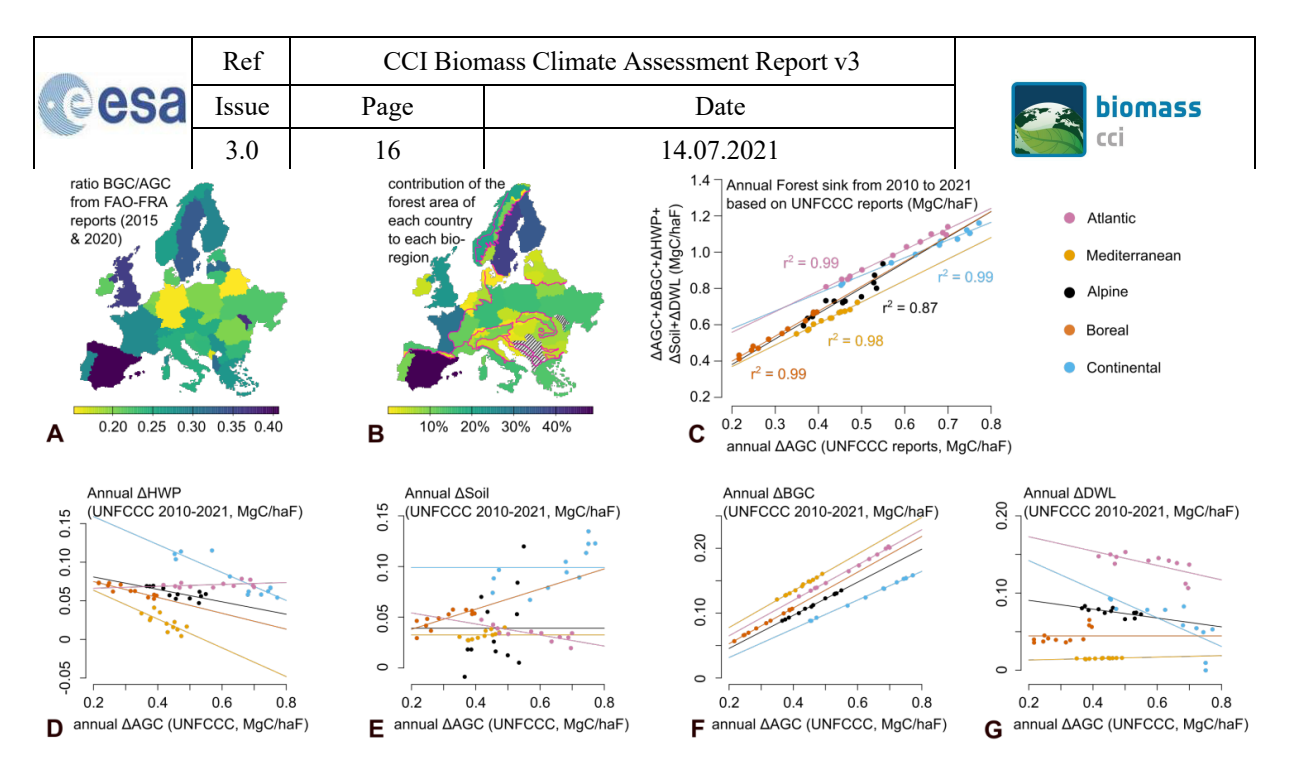


Figure 2-4 UNFCCC reports, computation of the BGC & AGC components, and linear relationships between forest sink components and annual changes in AGC. **A**, Ratio of belowground biomass (BGC) to AGC calculated based on the FAO-FRA reports of 2020 (the year 2015 has been used instead for Serbia, Albania, Portugal and Greece as the year 2020 was not yet available). This ratio is used to partition the annual carbon stock change in living biomass into the annual carbon stock change in AGC & BGC. **B**, Contribution of the forest area of each country to each bioregion, which allows to calculate each component of the forest sink (from the country reports to UNFCCC) for each biogeographical region. **C**, Linear relationships obtained from the UNFCCC reports associated with each biogeographical region of the forest sink FS (sum of annual carbon stock changes in AGC, BGC, Harvested Wood Products (HWP), Deadwood and Litter (DWL) and organic and mineral soil (soil)) versus annual carbon stock changes in AGC for 12 data points (years from 2010 to 2021). **D,E,F,G**, Similar relationships but for  $\Delta$ HWP,  $\Delta$ Soil,  $\Delta$ BGC and  $\Delta$ DWL versus  $\Delta$ AGC, respectively. The mean is calculated instead if the relationship is non-significant (p > 0.05).

#### 2.1.3 Future projection

To project the future forest carbon sink, we conservatively assumed that future disturbances would follow the same local trends as in the past 35 years while future AGC recovery curves would remain unchanged. Our projections for carbon sink trajectories are spatially explicit and can be aggregated at the national level for each EU-27 country. This allows comparison with the 2030 carbon sink target for the forest sector, which contributes to the broader land-use sector mitigation goal set by the European Commission. By partitioning harvests and natural disturbances based on their constant ratio at 18 km and adjusting the harvest trends in the DDCM, we infer the reduction in harvesting necessary to meet the 2030 target (while accounting for the observed increase in natural disturbances).

#### 2.2 Forest biomass recovery

Forest recovery after disturbance shows significant variations across different biogeographical regions of Europe <sup>20</sup> (Fig. 2-5A). In the Boreal region, forests typically need 118 [93,163] years on average to regain 90% of their maximum reachable AGC (AGC<sub>pot</sub>) after a stand-replacing disturbance event. The confidence intervals in brackets show the range obtained from model parameterization conducted on different AGC maps at different scales. Forests in the Atlantic

	Ref	CCI Biomass Climate Assessment Report v3	
esa	Issue	Page	Date
	3.0	17	14.07.2021



also take about a century to recover (101 [64,181] years), while recovery in the Alpine and Continental regions is twice as slow (239 [157,312] years). Their recovery is slower because it is defined here as a percentage of AGC<sub>pot</sub>, which is much higher in the Alpine and Continental regions (184 [162,223] MgC/haF, with haF standing for hectares of forest) compared to the Boreal and Atlantic regions (104 [85,147] MgC/haF). However, the Mediterranean region has the longest recovery time (more than 300 years) with the lowest potential AGC (72 [59,92] MgC/haF) due to it being water-limited. The accuracy of local recovery curves is confirmed by the small mean anomalies between satellite-derived and field-observed AGC (Fig. 2-5B) when the sample size is large enough for a given age. However, the precision of these curves is limited (large variability seen in the anomalies) due to the influence of varying factors (e.g., climate, soil, forest management) as well as the inherent uncertainties in *in situ* measurements.

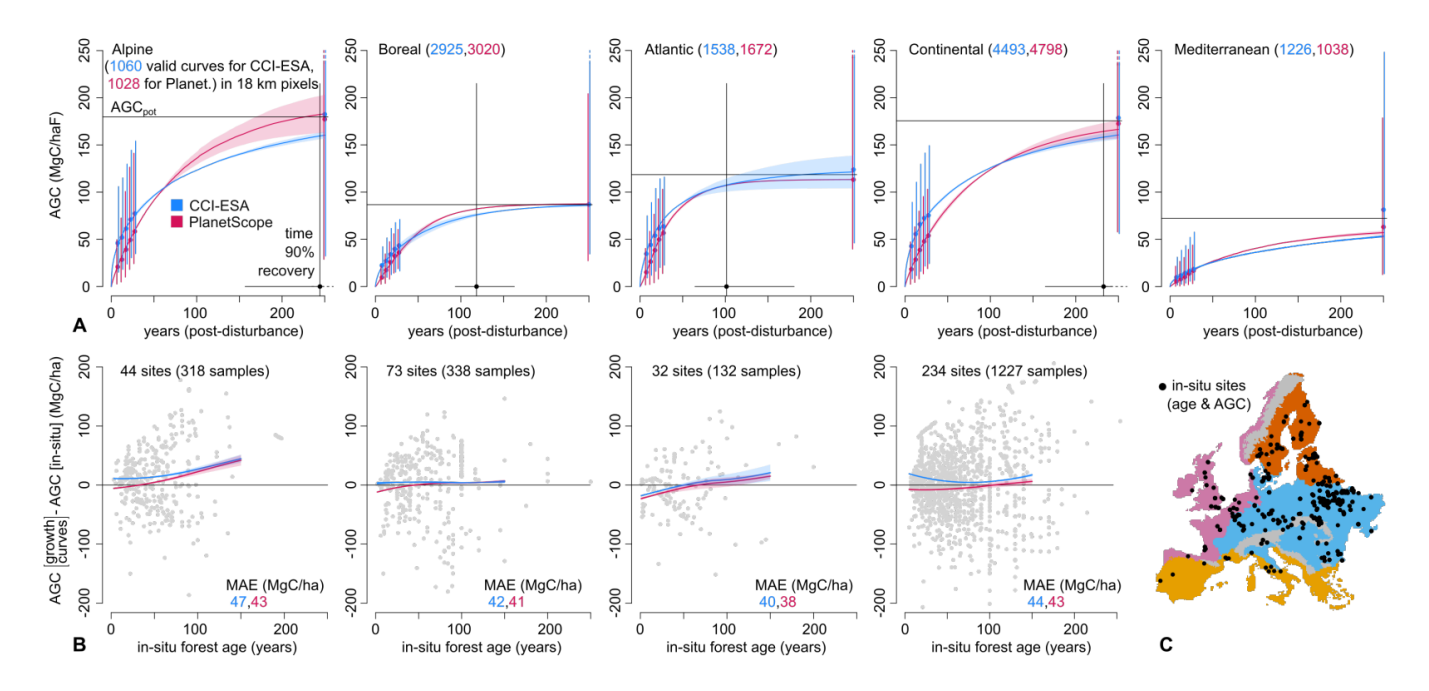


Figure 2-5 Forest growth in Europe. (A) AGC recovery curves computed at 18 km based on a Chapman-Richard equation:  $AGC_{CR}(t) = AGC_{pot}(1 - e^{-bt})^c$  using two AGB datasets (CCI-ESA in blue, and PlanetScope in red) harmonized with NFI data on a sub-national scale. See supplementary Fig. 2-6 for a map of coefficients b, c, and  $AGC_{pot}$ . The representative growth curve (thick line) is obtained with the median of all valid curves associated with a  $r^2 > 0.5$  in a specific biogeographical region. Points represent the median of the AGC after a stand-replacing disturbance (limited to 5-30 years based on the Landsat range) or the median of the potential AGC ( $AGC_{pot}$  displayed for the age = 250 years for visualization purposes only. AGC approaches  $AGC_{pot}$  asymptotically, never reaching it fully) across all 18 km pixels (whiskers show the 95% variability, from 2.5% to 97.5% percentile).  $AGC_{pot}$  is scaled from the AGC of forests undisturbed since 1986 with a bootstrap analysis that minimizes the difference between simulated and observed (UNFCCC) changes in AGC from 2010 to 2021. The 90% AGC recovery interval  $(t_{90})$  is retrieved at 18 km with  $AGC_{CR}(t_{90}) = 0.9AGC_{pot}$ , and then the median of all 18 km pixels is calculated. The shaded areas and the range of  $t_{90}$  (horizontal black line) represent the variability from the bootstrap conducted on the scale of a country or a biogeographical region. (B) In situ validation with the age and AGC of trees measured from 383 European sites. For each site,  $f_cAGC_{CR}(age) - AGC_{in \, situ}(age)$  has been computed using the nearest growth curve parameters, and  $f_c$  is the forest fraction estimated at 90 m around the site from our forest

	Ref	CCI Biomass Climate Assessment Report v3	
esa	Issue	Page	Date
	3.0	18	14.07.2021



mask. The thick curve represents the moving mean (loess) of all available anomalies, with a variability indicated by the mean absolute error for all available samples. The Mediterranean anomalies are discarded due to a small sample size (13 sites). (C) Location of the *in situ* sites and the biogeographical regions. The unit haF stands for hectares of forests.



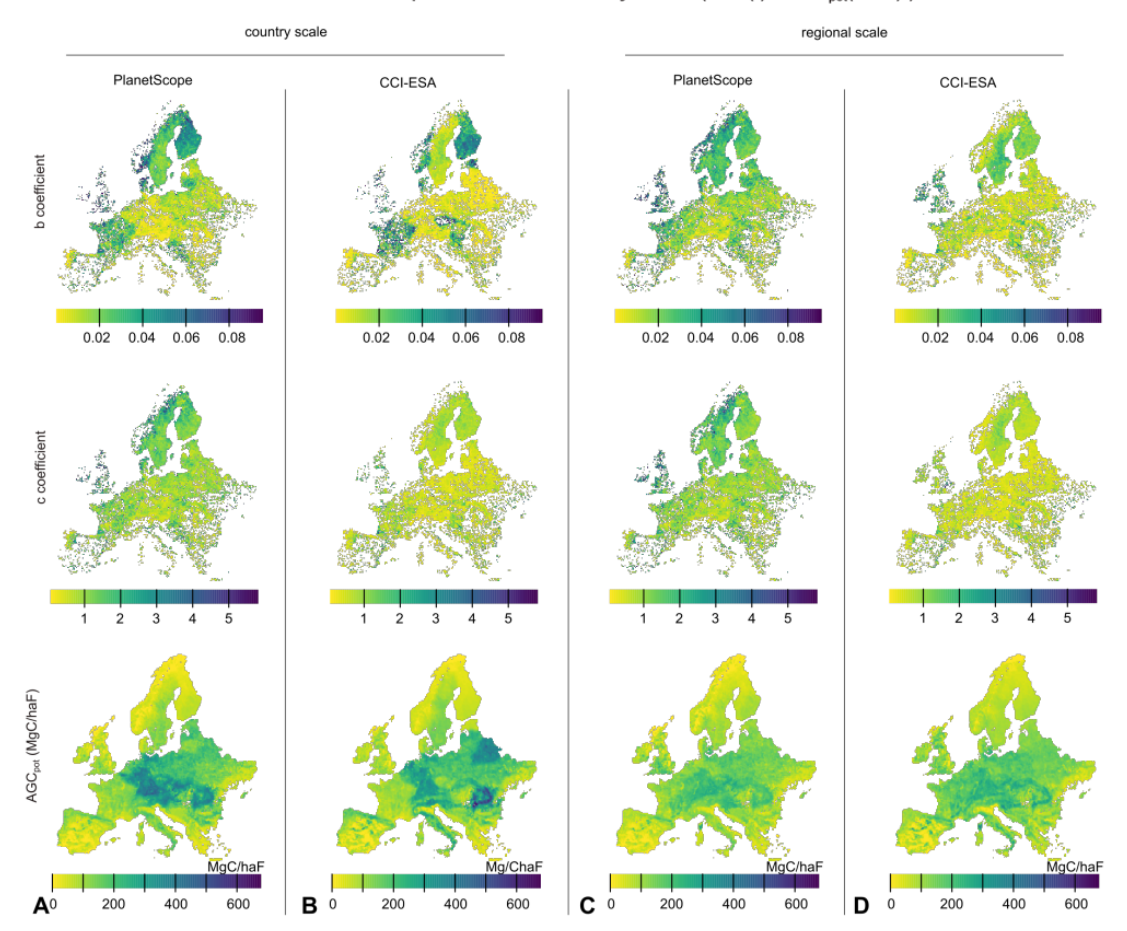


Figure 2-6 Chapman-Richards coefficients from the recovery curves. The Chapman-Richards growth function is decribed as  $AGC(t) = AGC_{pot}(1-e^{-bt})^c$ . **A.** Growth coefficients obtained from the parameterization of the DDCM at a country scale for the PlanetScope AGC map. **B.** Growth coefficients obtained from the parameterization of the DDCM at a country scale for the CCI-ESA AGC maps. **C.** Growth coefficients obtained from the parameterization of the DDCM at a regional scale for the PlanetScope AGC map. **D.** growth coefficients obtained from the parameterization of the DDCM at a regional scale for the CCI-ESA AGC maps. Missing values in these maps will be filled with spatial interpolations before simulating the AGC from 2010 to 2030.

#### 2.3 Carbon storage potential in a world without disturbance

On a global scale, studies have suggested that forests could significantly increase their biomass if allowed to regrow partially or fully <sup>24-28</sup>. We estimate that Europe could potentially increase its AGC stock by 15.8 [11.9,19.0] PgC, corresponding to a ~130% increase in AGC carbon stocks

	Ref	CCI Biomass Climate Assessment Report v3	
esa	Issue	Page	Date
	3.0	19	14.07.2021



relative to the period 2017-2020 (for the same forest area). This result is consistent with the conclusions of a recent study based on old-growth forests in Europe <sup>29</sup>. Being far from their saturation point, these forests reflect a broader shift in forest dynamics <sup>5,30</sup> characterized by a rapid increase in forest turnover rates. Mature forests steadily decline due to increased tree mortality, leading to significant ecological consequences <sup>31</sup>. Repeated disturbances affecting forests are not accounted for in these estimations, therefore the disturbance trends are implemented in the DDCM to provide more realistic projections of future AGC stocks (Fig. 2-7D).

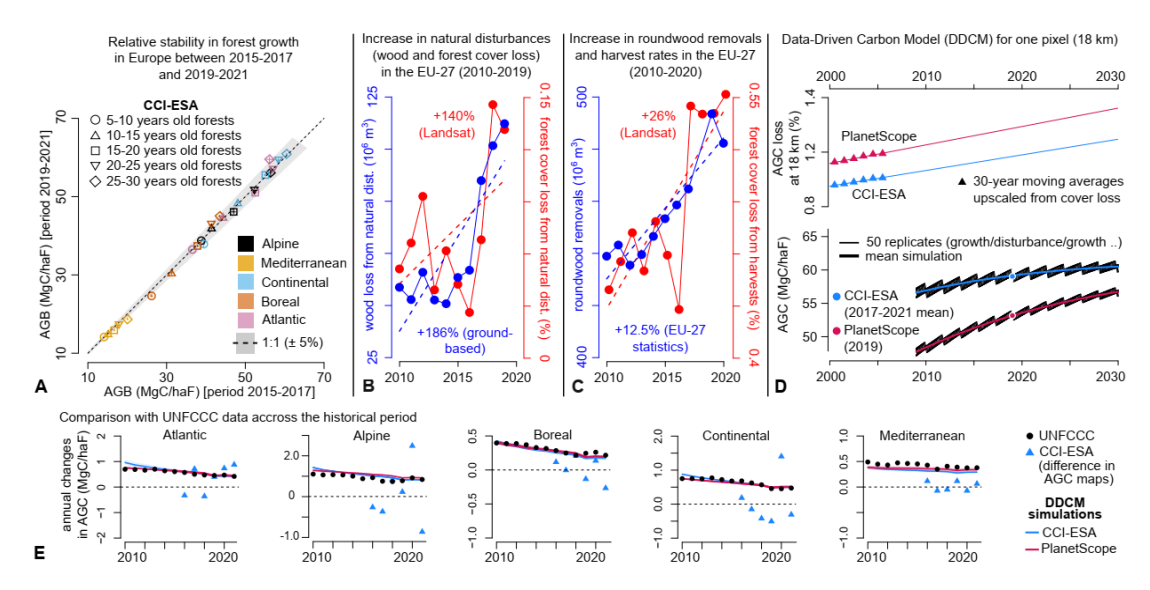


Figure 2-7. Changes in forest growth and disturbances, DDCM procedure, and remote sensing inconsistencies in biomass change. (A) Comparison across Europe of the mean AGC (CCI-ESA, bias-corrected with NFI data on a sub-national scale) of forests from 5 to 30 years old (Landsat range) between the periods 2015-2017 and 2019-2021. For each year (2015, 2016, 2017, 2019, 2020, 2021), the mean AGC of forests (for a given age class) has been aggregated from 30 m to 18 km. One point in panel A corresponds to the mean value of all 18 km pixels across Europe for the given period (2015-2017 for the X axis and 2019-2021 for the Y axis) and a given age class. (B) The volume of wood loss is shown in blue <sup>6</sup> and the percentage of forest cover loss is shown in red 8 due to natural disturbances in the EU-27 from 2010 to 2019. (C) Roundwood removals are shown in blue 32 and the percentage of forest cover loss is shown in red 8 due to harvest or salvage logging in the EU-27 from 2010 to 2020. The percentage of forest cover loss has been aggregated from the same sub-sample of Europe described in panel B. (D) Example of AGC simulations from the data-driven carbon model (DDCM) for a forested pixel at 18 km, from two AGC datasets (the year 2019 for PlanetScope and mean of 2017-2021 for CCI-ESA) and one parameterization (bootstrap conducted on each country). See Fig. 2-3 for more details. The simulated AGC is the mean of 50 replicates. For each replicate, the period of growth is equal to the return interval, which is the average time between two mean disturbances aggregated at 18 km across 30-year windows (typically between 1 and 5 years). Each replicate has a different starting time of the first disturbance. The mean percentage of AGC loss at 18 km is scaled from the mean percentage of forest cover loss with a bootstrap analysis that minimizes the difference between simulated and observed (UNFCCC) annual changes in AGC from 2010 to 2021. (E) Annual AGC changes from CCI-ESA maps (2015 to 2021), UNFCCC reports, and DDCM simulations from 2010 to 2021 (PlanetScope has only one year of data and changes cannot be assessed). Annual AGC changes for CCI-ESA (2016-2021) have been aggregated across each biogeographical region, regardless of the quality flag of the CCI-ESA product or possible 0 values emerging from a mismatch with our forest cover mask.

	Ref	CCI Biomass Climate Assessment Report v3	
esa	Issue	Page	Date
	3.0	20	14.07.2021



#### 2.4 Inconsistencies in biomass change detection using remote sensing

While the CCI-ESA biomass maps correctly capture the spatial variability of AGC (converted from AGB to AGC using a ratio of 0.5) among young, mature, and old forests (Fig. 2-5B), calculating AGC changes as the year-on-year difference between two consecutive AGC maps is unsuitable, as it produces AGC changes that are inconsistent with UNFCCC reports across the recent historical period (Fig. 2-7E, blue triangles versus black dots). For instance, this approach produces a net loss of AGC in the Continental region from 2017 to 2021 (except in 2020), contradicting the AGC accumulation reported by the UNFCCC for that period. In contrast, the AGC change simulations from the DDCM closely match UNFCCC data across all biogeographical regions (Fig. 2-7E). The NFI data used in the UNFCCC reports provide robust national-scale estimates of biomass carbon stock changes over time with a ~30% uncertainty <sup>35-38</sup>. However, they cannot provide insights into fine-scale spatial patterns; a gap effectively addressed by the DDCM that is spatially explicit (see next sections).

#### 2.5 Future carbon sink of Europe's forests

According to the DDCM, the net carbon sink of EU-27 forests is projected to decrease from 496 [459,521] MtCO<sub>2</sub>eq/year in 2010 to 279 [269,294] MtCO<sub>2</sub>eq/year by 2030 (Fig. 2-8A). This projection assumes that forest recovery curves remain unchanged in the near future (Fig. 2-5A) and that forest management and natural disturbances will continue linearly until 2030, following past trends observed in the mean percentage of AGC loss across 18 km grids (Fig. 2-7D). The largest decrease in the forest carbon sink is expected in the Boreal region, with a decline of 62%, while the Mediterranean region is predicted to maintain a stable sink. The forest carbon sink consists of five components, each with different significance and behavior (Fig. 2-8A). The net carbon stock change in living above- and below-ground biomass (ΔAGC + ΔBGC) will see a large decrease of 63% from 2010 to 2030 in the EU-27, which is the primary driver of the overall decline. However, this decline will be partially offset by increases in the net carbon stock changes of harvested wood products <sup>39</sup> (ΔHWP, +96%) and deadwood and litter resulting from recent disturbances (ΔDWL, +71%). The net carbon stock change in soils is expected to decrease by 17%, consistent with our current understanding of the impact of harvests on soil carbon dynamics <sup>40</sup>. While ΔHWP and ΔDWL only accounted for ~11% of the forest carbon sink in 2010, they are projected to contribute ~35% by 2030, acting as a temporary buffer against the declining carbon sink of living biomass and soils.

The resolution of the DDCM allows for the detailed computation of spatial variations in the AGC sink (Fig. 2-8B) in addition to the overall forest carbon budget (Fig. 2-8C) from 2010 to 2030. Regions such as Southern Germany, Northern Belarus, Northern Sweden, Southern Romania, Central Spain, the Pyrenees, and the Dinaric mountains are expected to continue to accumulate large proportions of AGC from 2010 to 2030 (Fig. 2-8B). These gains are attributed to either stationary or decreasing trends in disturbance levels (partly due to recovery from old disturbances like in Southern Germany), unlike other parts of the continent (Fig. 2-1B), where 12% of forests are projected to experience a net AGC loss (agreement between CCI-ESA and PlanetScope). Particularly, forests in Portugal, Slovenia, Southern France, Austria, Czechia, Estonia, Latvia, Northern Ukraine, Northern Germany, the Eastern Alps, and parts of Scandinavia are projected to face reductions in AGC (Fig. 2-8B). However, the impacts of these losses will be partially offset by increases in the net carbon stock changes in HWP and DWL (Fig. 2-8A), which will help compensate for the AGC loss in about half of these areas. Overall, our estimates indicate

	Ref	CCI Biomass Climate Assessment Report v3		Ī
esa	Issue	Page	Date	Ī
	3.0	21	14.07.2021	



that at least 6% of European forests will become net carbon sources between 2010 and 2030 (Fig. 2-8C, agreement between CCI-ESA and PlanetScope).

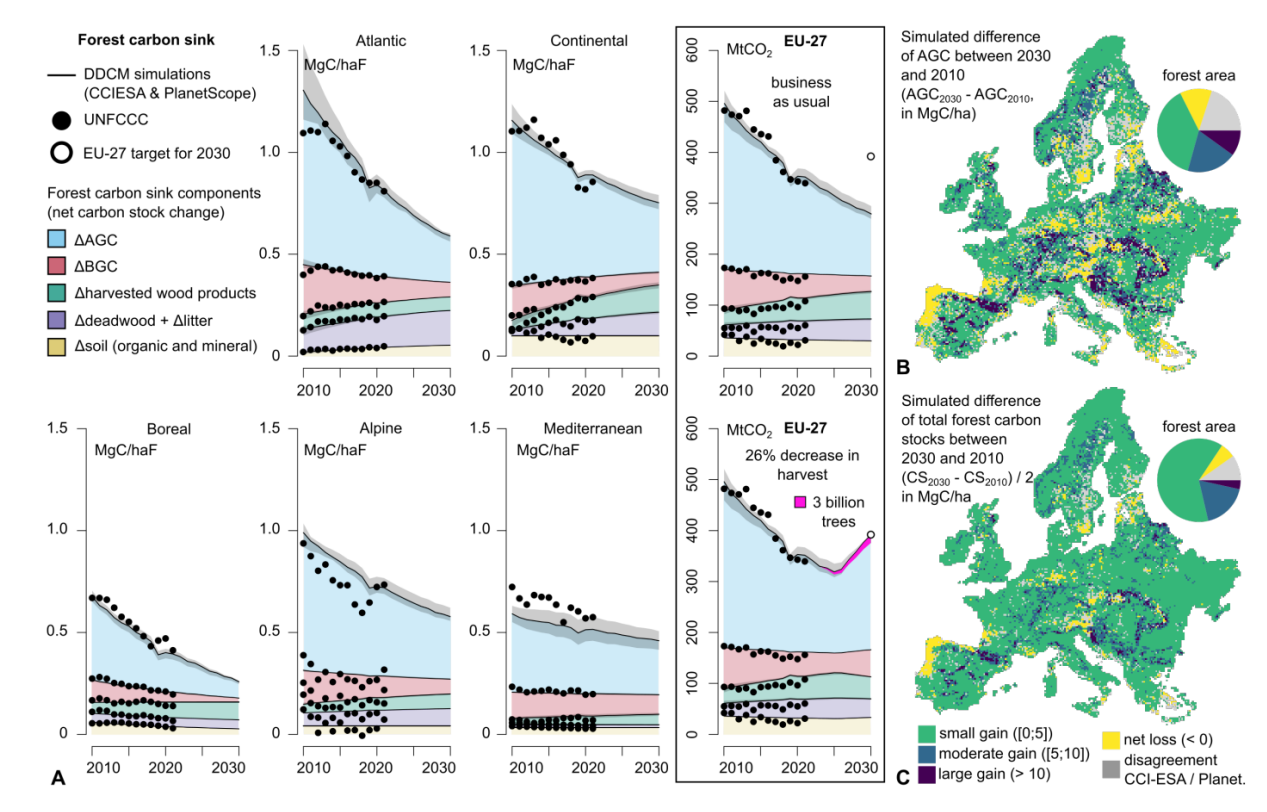
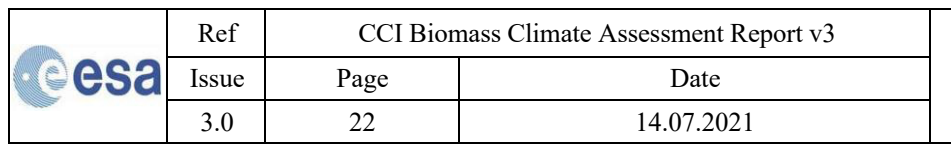


Figure 2-8 **Spatial and temporal changes in the carbon sink of European forests.** (**A**) Forest sinks for the five biogeographical regions and the EU-27 are based on two forest management scenarios: business as usual and a 26% decrease in harvest in addition to the 3 billion trees planted by 2030 (their total forest sink is pink). The forest sink is the sum of five components: net carbon stock change in the AGC, below-ground biomass (BGC), deadwood and litter, soils and harvested wood products. The EU-27 forest sink target has been estimated at 392 MtCO<sub>2</sub>eq, the average for the years 2016-2018. The black-shaded area represents the total variability obtained from using PlanetScope or CCI-ESA maps with the parameterization conducted per country or biogeographical region. (**B**) Map of the difference between 2030 and 2010 of the AGC simulated by the DDCM. Forests losing AGC from 2010 to 2030 are in yellow. (**C**) Map of the difference between 2030 and 2010 of the forest carbon stocks composed of AGC, BGC, deadwood and litter, soil and harvested wood products (values have been divided by 2 to match the legend). Forests losing carbon (acting as a source) from 2010 to 2030 are in yellow. For both panels **B** and **C**, inconsistencies between CCI-ESA and PlanetScope are in gray (when one product predicts a carbon source and the other a carbon sink).

#### 2.6 Challenges and mitigation strategies

A common assumption is that sustainable harvests carry a low carbon cost according to the rationale that (i) HWPs serve as a reliable long-term carbon sequestration asset, and (ii) young stands replacing mature forests are compensating for the carbon deficit because they are more productive <sup>41</sup>. Based on these premises, the EU-27 has endorsed wood use for bioenergy, which now represents 59% of renewable energy <sup>42</sup>. Regarding point (i), 69% of global HWPs have very





short lifespans, significantly reducing their contribution to the forest carbon sink <sup>41</sup>. For instance, estimates from the French NFIs show that 68% of HWPs are used as bioenergy <sup>43</sup>. Concerning point (ii), the DDCM demonstrates that the recovery of young and productive stands is insufficient to offset carbon losses from current natural and anthropogenic disturbances (Fig. 2-8A). These projections also address point (i) as they implicitly incorporate carbon transfers across different pools (especially HWPs and DWLs). The EU-27 plan could be made more effective by extending HWP lifespans (for example, using wood for construction material) and reducing wood use for bioenergy (by promoting other renewable energies) to lower harvest rates, especially as natural disturbances continue to increase dramatically (Fig. 2-7B). The impact of reducing harvest rates on the forest carbon sink is estimated below.

We estimate that the forest carbon sink of the EU-27 will be 29% lower than the 2030 sink target (forest state of 2016-2018), resulting in a carbon deficit of -113 MtCO2eq/year for the target sink in the forest sector. Despite the EU-27's plan to plant 3 billion trees by 2030, this initiative will only contribute an additional 15 MtCO2eq/year to the carbon sink 44, which is insufficient to close the gap. According to DDCM simulations, a 26 [20,31]% decrease in harvest from 2025 to 2030, in addition to the 3 billion new trees, would be sufficient for the EU-27 to reach the target (Fig. 2-8A). This estimate is a first-order assessment and should be refined in future studies by examining other forest management options than simply reducing harvest <sup>45,46</sup>. Forest biomass expansion could, for instance, be promoted by regenerating forests with thinning, changing rotations, considering biodiversity restoration versus monocultures, or choosing nonintervention versus salvage logging after a disturbance <sup>34</sup>. All these solutions need to be explored, as a continent-wide reduction in harvests will increase carbon market leakage, with harvests increasing outside Europe to meet European demand. Three recent studies predict that the forest sink values in 2030 will fall below the EU-27 target, based on different modeling approaches: large-scale simulations from a forestry carbon model (CBM) with business-as-usual forest management assumptions 46, multiple statistical extrapolations of current trends 39, and land-climate models under different Representative Concentration Pathway scenarios 47. Our data-driven model assumes that disturbances will evolve in the next six years as they did in the past, forecasting a less optimistic carbon sink for living biomass (ΔAGC and ΔBGC) than CBM predictions: 152 MtCO₂eq/year (DDCM) versus 240 MtCO₂eq/year (CBM) by 2030 for the EU-27. However, it is important to note that the CBM forestry model did not capture the recent declines in forest carbon sinks reported in the latest UNFCCC data from 2023 46.

Several limitations are acknowledged in our study. First, shifts in disturbance trends or changes in the growth rates of recovering forests <sup>19</sup>, whether due to natural or anthropogenic reasons, will impact the simulated trajectories. This is why we chose not to extend forecasts beyond 2030. Secondly, land-use changes such as deforestation and reforestation are not factored in, with the reasonable assumption that forest cover remains largely constant (only +1.6% increase from 2000 to 2021, Fig. 2-1D). Thirdly, we assumed that forests would continue to recover as they have in the past, regardless of disturbance frequency and severity (or increasing droughts). Notably, our model does not capture non-linear processes such as cascading effects in disturbance interactions (e.g., bark beetle outbreaks after a heatwave). This overlooks the potential for ecological tipping points <sup>12</sup>, beyond which the resilience of ecosystems is altered. Finally, the type and severity of disturbance (fires, storms, harvests) or the disturbance patch size, along with variations in forest structure (e.g., old versus young, coniferous versus deciduous, plantations versus natural forests), might change the way forests recover <sup>48</sup>. We plan to address these factors and their potential legacy effects in future studies.

	Ref	CCI Biomass Climate Assessment Report v3	
esa	Issue	Page	Date
	3.0	23	14.07.2021



#### 2.7 Conclusion

We present evidence that Europe's forests are increasingly at risk of losing their role as carbon sinks, primarily due to a dramatic increase in natural disturbances alongside a moderate increase in harvests. Although these forests have the potential to double their AGC stocks within the same forest area, disturbances are currently outpacing AGC recovery in 12% of European forests. Alarmingly, half of these endangered forests are projected to become net carbon sources by 2030. The carbon sequestration capacity of the remaining forests is progressively deteriorating, a trend exacerbated by business-as-usual forest management practices. Our projections for the near future are less optimistic than the EU-27's target, which will significantly impact European climate change mitigation plans that rely on increasing forest area. Over the past two decades, forest expansion has been limited. By November 2024, only 22 million trees had been planted in Europe <sup>49</sup>, falling short of the ambitious pledge to plant 3 billion trees by 2030. Even if this pledge were met, we estimate that a 26% decrease in forest harvest from 2025 to 2030 would be necessary for the EU-27 to reach their target. Historically, forest management in Europe has accumulated a substantial carbon debt <sup>50</sup>, further exacerbated by recent natural disturbances. To mitigate the decline in the European carbon sink, a major shift in forest management practices is essential, focusing on increasing resilience and better adapting to natural disturbances.

	Ref	CCI Biomass Climate Assessment Report v3	
esa	Issue	Page	Date
	3.0	24	14.07.2021



#### 2.8 Reference

- Fuchs, R., Herold, M., Verburg, P. H. and Clevers, J. G. A high-resolution and harmonized model approach for reconstructing and analysing historic land changes in Europe. *Biogeosciences* 10, 1543–1559(2013). https://doi.org/10.5194/bg-10-1543-2013
- 2. Avitabile, V., Pilli, R., Migliavacca, M. et al. Harmonised statistics and maps of forest biomass and increment in Europe. *Sci. Data* 11, 274 (2024). https://doi.org/10.1038/s41597-023-02868-8
- 3. European Commission. *Regulation (EU) 2023/839 of the European parliament and of the council Document no. 32023R0839* (Publications Office of the European Union, 2023). https://eurlex.europa.eu/legal-content/EN/TXT/?uri=celex%3A32023R0839.
- 4. Forest Europe. *State of Europe's Forests 2020* (Ministerial Conference on the Protection of Forests in Europe, 2020). https://foresteurope.org/wp-content/uploads/2016/08/SoEF\_2020.pdf
- 5. Senf, C., Sebald, J. and Seidl, R. Increasing canopy mortality affects the future demographic structure of Europe's forests. *One Earth4*, 749–755(2021). https://doi.org/10.1016/j.oneear.2021.04.008
- 6. Patacca, M. et al. Significant increase in natural disturbance impacts on European forests since 1950. *Glob. Chang. Biol.* **29**, 1359–1376(2023). https://doi.org/10.1111/gcb.16531
- 7. Van der Woude, A.M., Peters, W., Joetzjer, E. *et al.* Temperature extremes of 2022 reduced carbon uptake by forests in Europe. *Nat Commun*14, 6218 (2023). https://doi.org/10.1038/s41467-023-41851-0
- 8. Seidl, R., Senf, C. Changes in planned and unplanned canopy openings are linked in Europe's forests. *Nat Commun*15, 4741 (2024). https://doi.org/10.1038/s41467-024-49116-0
- 9. Overpeck, J. T., Rind, D. and Goldberg, R. Climate-induced changes in forest disturbance and vegetation. *Nature* **343**, 51–53(1990). https://doi.org/10.1038/343051a0
- 10. Senf, C. and Seidl, R. Mapping the forest disturbance regimes of Europe. *Nat. Sustain.* 4, 63–70(2021). https://doi.org/10.1038/s41893-020-00609-y
- 11. Senf, C. et al. Canopy mortality has doubled in Europe's temperate forests over the last three decades. *Nat. Commun.* 9, 4978(2018). https://doi.org/10.1038/s41467-018-07539-6
- 12. Forzieri, G., Dakos, V., McDowell, N. G., Ramdane, A. and Cescatti, A. Emerging signals of declining forest resilience under climate change. *Nature* 608, 534–539(2022). https://doi.org/10.1038/s41586-022-04959-9
- 13. Nabuurs, G.-J. et al. First signs of carbon sink saturation in European forest biomass. *Nat. Clim. Chang.* **3**, 792–796 (2013). https://doi.org/10.1038/nclimate1853
- 14. Anderegg, W. R. et al. Climate-driven risks to the climate mitigation potential of forests. *Science* **368**, eaaz7005 (2020). https://doi.org/10.1126/science.aaz7005
- 15. Winkler, K. et al. Changes in land use and management led to a decline in eastern Europe's terrestrial carbon sink. *Commun. Earth Environ.* 4, 237 (2023). https://doi.org/10.1038/s43247-023-00893-4
- Gschwantner, T. et al. Growing stock monitoring by European national forest inventories: Historical origins, current methods and harmonization. For. Ecol. Manag. 505, 119868 (2022). https://doi.org/10.1016/j.foreco.2021.119868
- 17. Santoro, M.; Cartus, O. (2024): ESA Biomass Climate Change Initiative (Biomass\_cci): Global datasets of forest above-ground biomass for the years 2010, 2015, 2016, 2017, 2018, 2019, 2020 and 2021, v5. NERC EDS Centre for Environmental Data Analysis, 22 August 2024. https://dx.doi.org/10.5285/02e1b18071ad45a19b4d3e8adafa2817
- 18. Liu, S. et al. The overlooked contribution of trees outside forests to tree cover and woody biomass across Europe. *Sci. Adv.*9, eadh4097 (2023). https://doi.org/10.1126/sciadv.adh4097
- 19. Petersson, H. et al. Individual tree biomass equations or biomass expansion factors for assessment of carbon stock changes in living biomass A comparative study. For. Ecol. Manag. 270, 78-84, doi:https://doi.org/10.1016/j.foreco.2012.01.004 (2012).
- 20. Pretzsch, H., et al. Forest growth in Europe shows diverging large regional trends. Sci Rep 13, 15373 (2023). https://doi.org/10.1038/s41598-023-41077-6
- 21. Heinrich, V.H.A. et al. The carbon sink of secondary and degraded humid tropical forests. *Nature***615**, 436–442 (2023). https://doi.org/10.1038/s41586-022-05679-w
- 22. Besnard, S. et al. Mapping global forest age from forest inventories, biomass and climate data. Earth Syst. Sci. Data. 13, 4881–4896 (2021). https://doi.org/10.5194/essd-13-4881-2021

	Ref	CCI Bion	nass Climate Assessment Report v3
esa	Issue	Page	Date
	3.0	25	14.07.2021



- 23. Ceccherini, G. et al. Abrupt increase in harvested forest area over Europe after 2015. *Nature* **583**, 72–77(2020). https://doi.org/10.1038/s41586-020-2438-y
- 24. Ciais, P. et al. Carbon accumulation in European forests. *Nat. Geosci.* **1**, 425–429(2008). https://doi.org/10.1038/ngeo233
- 25. Verkerk, P. J. et al. Spatial distribution of the potential forest biomass availability in Europe. *For. Ecosys.* **6**, 1–11 (2019). https://doi.org/10.1186/s40663-019-0163-5
- 26. Cook-Patton, S. C. et al. Mapping carbon accumulation potential from global natural forest regrowth. *Nature* **585**, 545–550(2020). https://doi.org/10.1038/s41586-020-2686-x
- 27. Roebroek, C. T., Duveiller, G., Seneviratne, S. I., Davin, E. L. and Cescatti, A. Releasing global forests from human management: How much more carbon could be stored? *Science* **380**, 749–753(2023). https://doi.org/10.1126/science.add5878
- 28. Mo, L., Zohner, C.M., Reich, P.B. et al. Integrated global assessment of the natural forest carbon potential. *Nature* (2023). https://doi.org/10.1038/s41586-023-06723-z
- 29. Keith, H., Kun, Z., Hugh, S. et al. Carbon carrying capacity in primary forests shows potential for mitigation achieving the European Green Deal 2030 target. *Commun Earth Environ*5, 256 (2024). https://doi.org/10.1038/s43247-024-01416-5
- 30. McDowell, N. G. et al. Pervasive shifts in forest dynamics in a changing world. *Science* **368**, eaaz9463(2020). https://doi.org/10.1126/science.aaz9463
- 31. Hua, F. et al. The biodiversity and ecosystem service contributions and trade-offs of forest restoration approaches. *Science* 376, 839–844 (2022). https://doi.org/10.1126/science.abl4649
- 32. Eurostat, Roundwood removals by type of wood and assortment. https://doi.org/10.2908/FOR\_REMOV. Last data access: 25/10/2024.
- 33. Memento (édition 2024) de l'inventaire forestier national. https://www.ign.fr/publications-de-lign/institut/kiosque/publications/docs\_thematiques/memento-2024.pdf
- 34. Müller, Jörg, et al. Increasing disturbance demands new policies to conserve intact forest. *Conservation Letters* **12(1)**, e12449 (2019). https://doi.org/10.1111/conl.12449
- 35. Phillips, D. L., Brown, S. L., Schroeder, P. E. and Birdsey, R. A. Toward error analysis of large-scale forest carbon budgets. *Glob. Ecol. Biogeogr.*9, 305–313 (2000). https://doi.org/10.1046/j.1365-2699.2000.00197.x
- 36. Grassi, G. et al. Carbon fluxes from land 2000-2020: Bringing clarity to countries' reporting. *Earth Syst. Sci. Data* **14**, 4643–4666(2022). https://doi.org/10.5194/essd-14-4643-2022
- 37. McGlynn, E., Li, S., Berger, M. F., Amend, M. and Harper, K. L. Addressing uncertainty and bias in land use, land use change, and forestry greenhouse gas inventories. *Clim. Change* **170**, 5(2022). https://doi.org/10.1007/s10584-021-03254-2
- 38. Yu, Y. et al. Making the US National Forest Inventory spatially contiguous and temporally consistent. *Environ. Res. Lett.* **17**, 065002 (2022). https://doi.org/10.1088/1748-9326/ac6b47
- 39. Hyyrynen, M., Ollikainen, M. and Seppala, J. European forest sinks and climate targets: past trends, main drivers, and future forecasts. *Eur. J. For. Res.* 142, 1–18(2023). https://doi.org/10.1007/s10342-023-01587-4
- 40. Mayer, M., et al. Tamm Review: Influence of forest management activities on soil organic carbon stocks: A knowledge synthesis. Forest Ecol. Manage. 466, 118127 (2020). https://doi.org/10.1016/j.foreco.2020.118127
- 41. Peng, L., Searchinger, T.D., Zionts, J. et al. The carbon costs of global wood harvests. Nature 620, 110–115 (2023). https://doi.org/10.1038/s41586-023-06187-1
- 42. European Commission: Directorate-General for Energy, Union bioenergy sustainability report Study to support reporting under Article 35 of Regulation (EU) 2018/1999 Final report, Publications Office of the European Union, 2024, https://data.europa.eu/doi/10.2833/527508
- 43. Les forêts françaises face au changement climatique. Rapport du Comité des sciences de l'environnement de l'Académie des sciences et points de vue d'Académiciens de l'Académie d'Agriculture de France. June, 2023. https://www.academie-sciences.fr/pdf/rapport/rapport\_forets\_v2\_LD.pdf
- 44. Grassi, G., et al., Brief on the role of the forest-based bioeconomy in mitigating climate change through carbon storage and material substitution. Sanchez Lopez, J., Jasinevičius, G. and Avraamides, M. editor(s),

	Ref	CCI Biomass Climate Assessment Report v3	
esa	Issue	Page	Date
	3.0	26	14.07.2021



European Commission, JRC124374 (2021). https://publications.jrc.ec.europa.eu/repository/handle/JRC124374

- 45. Kauppi, P. E. et al. Carbon benefits from Forest Transitions promoting biomass expansions and thickening. *Glob. Change Biol.* 26, 5365-5370 (2020). https://doi.org/10.1111/gcb.15292
- 46. Korosuo, A., Pilli, R., Abad Viñas, R. et al. The role of forests in the EU climate policy: are we on the right track?. *Carbon Balance Manage*. 18, 15 (2023). https://doi.org/10.1186/s13021-023-00234-0
- 47. Pilli, R., Alkama, R., Cescatti, A., Kurz, W. A. and Grassi, G. The European forest carbon budget under future climate conditions and current management practices. *Biogeosci.* 19, 3263-3284(2022). https://doi.org/10.5194/bg-19-3263-2022
- 48. Babst, F. et al. Twentieth century redistribution in climatic drivers of global tree growth. *Sci. Adv.* **5**, eaat4313(2019). https://doi.org/10.1126/sciadv.aat4313
- 49. Forest Information System in Europe (9 November, 2024). https://forest.eea.europa.eu/3-billion-trees/introduction
- 50. Naudts, K. et al. Forest management: Europe's forest management did not mitigate climate warming. *Science* **351**, 597–600(2016). https://doi.org/10.1126/science.aad7270

	Ref	CCI Biomass Climate Assessment Report v3	
esa	Issue	Page	Date
	3.0	27	14.07.2021



## 3. Disturbance-recovery dynamics drive global forest biomass change

Forests constitute the largest carbon reservoirs in the terrestrial biosphere. The capacity of forests to sequester and store carbon is closely linked to their age structure, disturbance regimes, and post-disturbance recovery dynamics <sup>1,2</sup>. However, increasing anthropogenic pressures and climate-related extremes are intensifying the frequency, extent, and severity of forest disturbances <sup>3</sup>. These disturbances, including wildfires, insect outbreaks, storms, and logging, although not necessarily resulting in forest land-use change, can alter forest structure, disrupt carbon dynamics, and threaten the long-term stability of the terrestrial carbon sink.

Recent advances in Earth observation (EO) have substantially enhanced our ability to monitor forest disturbances across large spatial and temporal scales. In particular, the Landsat satellite archive provides a continuous multi-decadal record that enables the reconstruction of disturbance histories and the modeling of post-disturbance forest recovery. Several satellite-derived datasets now track forest age dynamics <sup>4–6</sup>, but their spatial coverage remains limited. The recently updated Global Age Mapping Inventory (GAMIv2.0) represents a notable improvement, refining spatial resolution from 1 km to 100 m by integrating Landsat-derived stand-replacement events over the past two decades <sup>7,8</sup>. Nevertheless, it tends to overestimate the age of younger forests, due to the lack of disturbance records before the 2000s and the omission of non-stand-replacing events <sup>7</sup>. These limitations constrain our ability to fully characterize forest age structures and disturbance patterns <sup>5,6,9</sup>, which are critical for accurately quantifying the spatial and temporal patterns of aboveground carbon (AGC) fluxes and understanding forest carbon recovery trajectories.

Despite these observational advances in forest monitoring, integration with existing modeling frameworks remains limited, as current models often fail to fully utilize the spatiotemporal detail available in EO products. Bookkeeping models (BMs) 10-12, as used in the Global Carbon Budget (GCB), were originally developed to estimate land-use change emissions and rely on prescribed carbon densities and fixed temporal response curves tied to specific land-use transitions. These models are driven by historical land-use reconstructions and generally exclude natural disturbances and forest age dynamics. In contrast, process-based Dynamic Global Vegetation Models (DGVMs), which are used in the GCB framework to quantify gross forest carbon uptake, often lack explicit representation of age-dependent growth processes and the disturbanceinduced carbon losses such as wildfire, windthrow, and insect outbreaks 13,14. National Greenhouse Gas Inventories (NGHGIs), which follow IPCC guidelines, offer a bottom-up alternative but differ conceptually from global models by including indirect effects on managed lands and broader definitions of anthropogenic influence <sup>15</sup>. Collectively, these approaches have provided critical insights into forest carbon dynamics, yet they show substantial discrepancies in the treatment of forest extent (e.g., definitions of managed land), representation of disturbance types, and the attribution of indirect effects such as CO₂ fertilization and climate variability. These inconsistencies result in divergent estimates of forest carbon fluxes and hinder reconciliation between observational data and model outputs. As such, there is an increasing need for spatially explicit approaches that directly link observed disturbance histories with biomass changes to improve model-data consistency.

	Ref	CCI Biomass Climate Assessment Report v3	
esa	Issue	Page	Date
	3.0	28	14.07.2021



In this study, we address this gap by integrating global and region-specific datasets of forest disturbance and biomass. We examine how historical disturbances during the Landsat era have shaped current forest age structures and influenced carbon dynamics across eight major global regions: Canada, Europe, other boreal regions, the United States, China, the tropics, Australia, and the remaining areas. By coupling a spatially explicit carbon bookkeeping framework with gridded forest biomass recovery curves, we aim to: (1) quantify forest AGC changes associated with fire and non-fire disturbances, (2) evaluate the regional contributions to the global forest carbon budget, and (3) assess carbon residence times under prevailing disturbance regimes.

#### 3.1 Method

#### 3.1.1 Delineation of forest disturbances

We separated the global forested area into 8 subregions, including Canada, Europe, other boreal regions, the United States (mainland), China, the tropics, Australia, and other remaining regions (**Fig. 3-2c**). The 8 regions were delineated due to the availability of disturbance datasets (**Table 3-1**), which are introduced in detail in the following paragraphs.

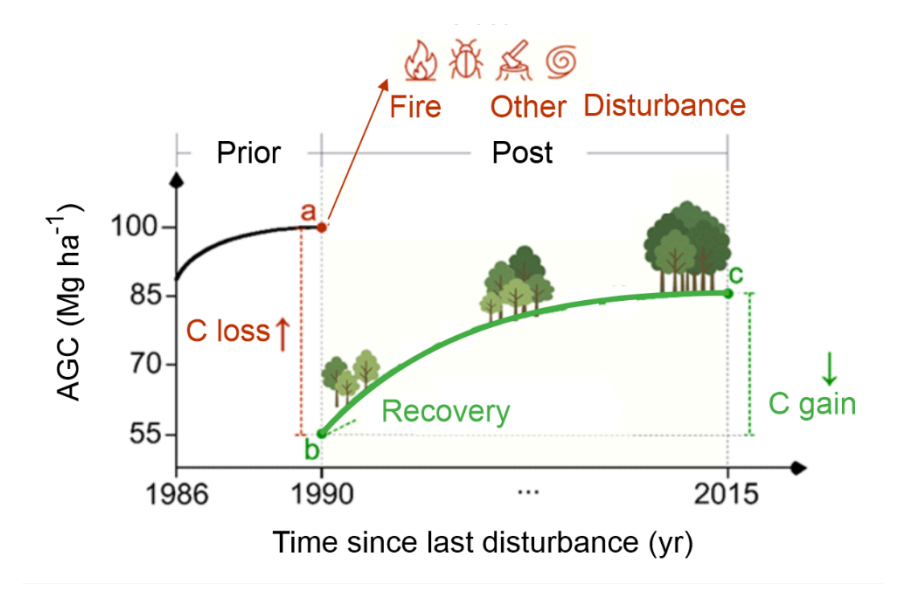


Figure 3-1 Conceptual diagram

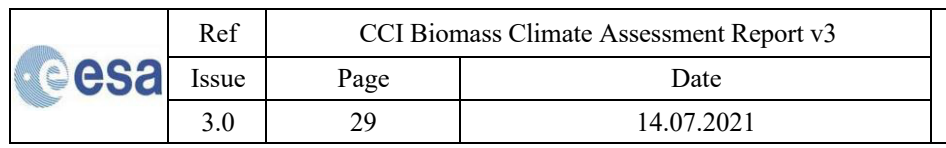


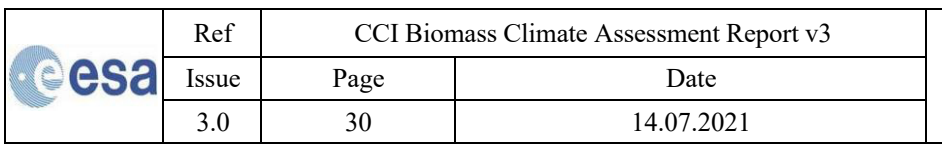


Table 3-1 Disturbance datasets used in the analysis

Dogion	Time Devied	Original type	Harmonized	Dataset Name	Reference
Region	Time Period	Original type	disturbance type		Reference
Canada	1985-2020	Harvest, fire	Fire, Non-fire	Canada's disturbance datasets	Hermosilla et al. (2019) <sup>16,17</sup>
Europe	1985-2023	Wind/bark beetle, fire, harvest	Fire, Non-fire	European Forest Disturbance Atlas (EFDA)	Viana-Soto and Senf (2025) <sup>18</sup>
US	1985-2020 1985-2015	Fire, other	Fire, Non-fire	Monitoring Trends in Burn Severity (MTBS) Disturbance intensity	USGS (2023) Lu et al., (2023) <sup>19</sup>
China	1986-2022	Fire, other	Fire, Non-fire	China's disturbance datasets	Liu et al., (2023) <sup>20</sup>
Tropics	1990-2023	Degradation, deforestation, Regrowth. Fire	Humid: Fire, Non-fire Dry: Fire	Tropical Moist Forest (TMF) Global Annual Burned Area datasets	Vancutsem et al., (2021) Long et al., (2021) <sup>21,22</sup>
Australia	1988-2023	Original land cover class: woody, forest, other	Fire, Non-fire (forest loss/gain)	National Forest and Sparse Woody Vegetation Data	Department of Climate Change, Energy, the Environment and Water (2023) Long et al., (2021) <sup>21</sup>
Other boreal/ Other	1985-2021	Burned area	Fire	Global Annual Burned Area datasets (GABAM)	Long et al., (2021) <sup>21</sup>

**Canada:** We used the disturbance datasets developed by <sup>16</sup> for Canada, which provides a spatially explicit, yearly record of stand-replacing forest disturbances from 1985 to 2020. This Landsat-based dataset distinguishes between wildfire and harvest disturbances and was generated using the automated Composite2Change (C2C) algorithm <sup>17</sup>. The year of forest change was identified by applying a segmentation algorithm to time series of the Normalized Burn Ratio (NBR), derived from Landsat surface reflectance data, followed by classification of disturbance types using object-based image analysis and a random forest model. The dataset achieved an overall change detection accuracy of 89% <sup>17</sup>.

**Europe:** For Europe, we utilized the European Forest Disturbance Atlas (EFDA) <sup>18</sup>, which provides annual, spatially explicit forest disturbance maps across 38 European countries from 1985 to 2023. The EFDA offers detailed information on the disturbance occurrence, severity (calculated using spectral changes in the Normalized Burn Ratio, NBR), and type, which is categorized into wind/bark beetle, fire, and harvest. The disturbance dataset is derived based on a consistent summer Landsat composite data cube and a classification-based approach capable of identifying both single and multiple disturbance events. EFDA reports an overall F1 accuracy score of 0.89, with commission and omission errors of 17.3 % and 22.5 % for the disturbed forest areas and omission errors of less than 1% for undisturbed forest areas, supporting robust detection and





attribution of forest disturbances. The disturbances are further grouped into fire and other non-fire disturbances (including wink/bark beetle and harvest).

The United States: For the United States, an annual disturbance intensity map (30 m, 1986-2015) from <sup>19</sup> and fire records from Monitoring Trends in Burn Severity (MTBS) (30 m, 1984-2024) <sup>23</sup> were used. The disturbance intensity map provides estimates of forest disturbance intensity across the conterminous United States. The MTBS includes both wildfires and prescribed fires that meet defined thresholds (1,000 acres or greater in the western US and 500 acres or greater in the eastern US) occurred in forest and non-forest area. To delineate forest fires, we overlapped the fire records with the Land Use/Land Cover Change layer (30 m, 1985-2023, USGS et al. (2025)) and extracted the burned pixels within the forest area. We overlaid the forest fires and disturbance intensity map and classified the pixels into two categories: fire and other non-fire disturbances. Any disturbance pixel that does not overlap with a fire pixel was classified as "other non-fire disturbances".

China: We used the forest disturbance dataset developed by Liu et al. (2023)<sup>20</sup>, which provides a spatially explicit, annual record of forest disturbances from 1986 to 2020 for China. This disturbance product was generated using the growing season (June–September) Landsat imagery. A LandTrendr spectral-temporal segmentation algorithm was applied to multiple spectral indices to characterize forest and change conditions. Forest disturbance were classified into fire and non-fire categories using a random forest model trained on over 31,000 reference points. The year of disturbance was assigned with an accuracy of ±3 years and the overall classification achieved an accuracy of 88.2%.

Tropics: The tropical area covers the same study domain as the tropical moist forest (TMF) datasets (Vancutsem et al. 2021)<sup>22</sup>, which approximately overlaps the 'Tropical rainforest,' 'Tropical moist forest,' 'Tropical mountain system' and 'Tropical dry forest' zones from the FAO global ecological zones. We used pixels belonging to the classes of forest cover and changes from the TMF Transition Map to define the humid forest extent. For the dry forest, we delineated the extent by removing the humid forest extent from a global tree cover map (Hansen et al. 2013)<sup>29</sup> for the year 2000 with a tree cover threshold of >25% following Hansen et al. (2010). The TMF dataset provide 33 yearly change maps, which categorised the disturbances across humid tropics into degradation, deforestation, and regrowth following deforestation. Deforestation in TMF refers to the change of land use from forest to non-forest areas or a loss of canopy cover without subsequent recovery over the past 3 years (Vancutsem et al. 2021)<sup>22</sup>. Forest degradation is not accompanied by permanent land use change (LUC) but is related to a decline in canopy cover and biomass. Forest degradation was defined following TMF datasets as a short-term disturbance (shorter than 2.5 years) followed by forest recovery. These degradations were caused by logging, windbreaks and droughts. Forest regrowth refers to forests regrowing following deforestation or afforestsation from non-forested land. The TMF reports an overall accuracy of 91.4%, with omission and commission errors for non-forest cover detection at 9.4% and 7.9%, respectively (Vancutsem et al. 2021)<sup>22</sup>. We further overlapped global annual burned area map (Long et al., 2019)<sup>21</sup> with the TMF annual change maps, to extract the fire and non-fire disturbance in humid troipcs. Deforestation without regrowth and afforestation is not accounted in this analysis for the aim of targeting forest disturbance in the established forest stands without land use change. Due to the lack of disturbance dataset in dry tropics, we overlapped the dry tropical forest extent in 2020 with the global annual burned area map (Long et al., 2019)<sup>21</sup> to delineate the fire disturbance historically occurred in dry tropical forests. The dry tropical forest extent in 2020 was derived from the dry forest extent in 2000 by excluding the tree cover loss pixels during 2000-2020 from Hansen et al. (2013) $^{29}.$ 

esa	Ref	CCI Biomass Climate Assessment Report v3		
	Issue	Page	Date	
	3.0	31	14.07.2021	Ī



Australia: The National Forest and Sparse Woody Vegetation Data (Version 8.0 - 2023 Release) provides an annual consistent discrimination between forest, sparse woody, and non-woody land cover across Australia from 1988 to 2023 at ~30 m resolution. The 'forest' is defined as woody vegetation with a minimum 20% canopy cover, at least 2 meters high, and a minimum area of 0.2 hectares, while 'sparse woody' is defined as woody vegetation with a canopy cover between 5-19%. The methodology employs time series processing using conditional probability networks to detect woody vegetation cover based on Landsat time series. To delineate the forest disturbances, we extract the forest loss from the land cover time-series with the change from forest to woody/non-woody and forest gain from woody/non-woody to forest. When the 30m forest loss pixels overlapped with the fire pixels at the corresponding year from the global annual burned area dataset (Long et al., 2019)<sup>21</sup>, these pixels were assigned as the fire-induced forest losses and the remaining ones were attributed to other non-fire losses.

**Other boreal and Other:** For the remaining regions without detailed disturbance datasets, the global annual burned area map derived from Landsat images was used (1985-2021)<sup>21</sup>. The burned area dataset contains a 8-year gap for the pre-2000 period due to the limited Landsat data availability. The accuracy of fire products of 2015-2019 was assessed with the stratified random sampling method, and the accuracy validation results show the accuracy of GABAM products in different years (2015-2019) was relatively stable, with overall accuracy ranging from 86.00% to 93.92%, Commission Error from 4.13% to 13.17%, and Omission Error from 29.81% to 34.86% <sup>21</sup>. We overlapped the burned area with forest cover map and forest loss map from global forest watch (Hansen et al., 2013)<sup>29</sup> to delineate the forest fires from the original burned area dataset. We further separate these burned forests into two regions, the other boreal regions (e.g., Alaskan and Russiaian boreal forests) and the other remaining regions.

Globally, the forest disturbances were separated into the fire and other non-fire disturbances, except for the other boreal and the other remaining regions, where other non-fire disturbance at the temporal depth of Landsat are not available at the moment. It is also important to notice that only forest disturbances happened in the existing forest stands were included in the analysis, whereas forest land use change (such as deforestation or afforestation) was excluded, due to inconsistency between the different land cover datasets.

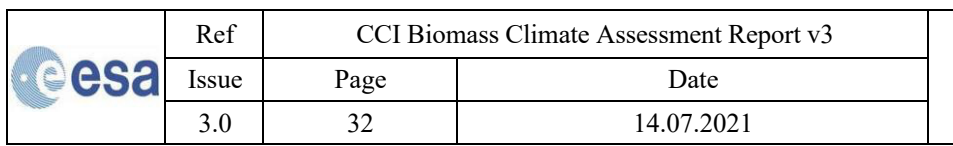
#### 3.1.2 Biomass dataset

#### Global above-ground biomass dataset

We used the ESA Climate Change Initiative Biomass dataset (CCI-Biomass v5 <a href="https://climate.esa.int/en/projects/biomass/data/">https://climate.esa.int/en/projects/biomass/data/</a>) to model forest carbon changes. This dataset provides global aboveground biomass (AGB) estimates for multiple years at 100 m spatial resolution. AGB values are derived from a fusion of Earth observation data, including radar signals from Copernicus Sentinel-1, Envisat ASAR, and JAXA's ALOS-1 and ALOS-2 sensors. Importantly, the dataset incorporates updated allometric relationships informed by an extended record of spaceborne LiDAR measurements from the GEDI and ICESat-2 missions. To ensure spatial consistency with the forest disturbance dataset, the CCI-Biomass map was resampled to 30 m resolution using nearest-neighbor interpolation.

#### Other regional biomass dataset

Two additional regional biomass datasets at 30m resolution were used, which better matched the original resolution of the disturbance datasets.





For Canadian forests, we used the biomass dataset developed for northern boreal ecosystems from <sup>24</sup> at 30m. AGB was modeled through a machine learning approach (XGBoost) by fusing ICESat-2-derived canopy structure metrics and Sentinel-2 spectral indices. The dataset was trained and validated using the AGB values from national forest inventories (NFI) in Finland, Sweden, and Norway. Validation showed strong agreement with reference data, with RMSE values around 33–43 Mg/ha across countries.

For Europe, we used the biomass dataset developed by <sup>25</sup>, which estimates aboveground biomass (AGB) by integrating PlanetScope imagery with deep learning models. These models predict tree canopy cover and height, which are then converted to AGB at 30m resolution using allometric equations derived from Danish NFI plots. The dataset captures biomass for both forest and non-forest trees. Validation against independent field measurements and national inventory data showed a systematic bias of +7.6% and a Pearson correlation coefficient of 0.98 at the country level.

#### 3.1.3 Model the forest carbon gain and losses for the disturbed forest

#### Identification of the forest age

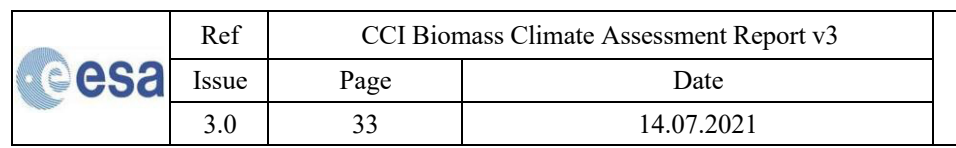
We first identified the forest age in 2020 since the last disturbance for each 30m pixel based on the regional disturbance history. If multiple disturbances occurred in the same 30m pixel, the most recent disturbance was used to calculate the forest age in 2020. For example, if a pixel experienced fire or non-fire disturbances in both 1990 and 1995, the year 1995 event was taken as the reference point (i.e., the year since the last disturbance), resulting in a forest age of 26 years in 2020, assuming that recovery begins in the same year as the disturbance.

#### Reconstruction of the post-disturbance recovery curves

To quantify the relationship between aboveground carbon (AGC, converted from AGB using a ratio of 0.5) and forest age (i.e., time since the last disturbance), we employed a space-for-time substitution approach. Specifically, we overlapped satellite-derived biomass maps with forest age maps to extract AGC-age pairs within each 1°×1° spatial window. Due to the temporal extent of the remote sensing disturbance data (beginning in 1985), the maximum observable forest age is currently limited to 36 years. To extend the AGC-age relationship beyond this range, data from the NFIs (Besnard et al., 2021)<sup>33</sup> were incorporated during the fitting process, providing additional AGC-age observations for older forest stands. If no NFI data were available for a 1°×1° grid cell, an estimated data point was added at a forest age of 200 years, with the corresponding AGC set to 85% of the maximum AGC within that grid cell. 85th percentile was chosen to minimize the differences (mean differences of 1.2 MgC ha<sup>-1</sup>) at the gridded level between the AGC density of the intact forest by overlapping the 2020 intact forest layer (Potapov et al., 2019)<sup>26</sup> and the gridded AGC maps. For each 1°×1° grid cell, the median AGC values and the corresponding ages were used to fit the biomass recovery curves following Richard-Chapman functions.

$$AGC_{ti+1} = AGC_{max}(1 - e^{-bti})^c + d \tag{1}$$

where  $AGC_{max}$  denotes asymptotic AGC, which determines the maximum potential AGC the forest could reach and ti refers to the time since the last disturbance. Parameters b, c, and d denote the recovery curves' rate, shape, and intercept.





The recovery curves were derived for each grid cell across global forests, considering two types of disturbances, fire-disturbance and other non-fire disturbances. In the case of Canada, stand-replacing disturbances were detected  $^{16}$ , the forests are assumed to regrow from zero tree cover, and d equals 0. For other non-stand-replacing disturbances where only partial AGC is removed, d represents the remaining AGC after disturbances.

We tested alternative growth functions for regrowth forests, including the Michaelis-Menten  $(AGC_{ti+1} = a \times ti/(b+x))$  and Logistic models  $(AGC = a/(1+be^{-c\times ti}))$ . These alternatives produced similar AGC accumulation patterns, suggesting that our estimates are robust to the choice of model forms within the relevant timeframe. The fitting performance improved with increasing grid sizes from 0.25° to 1° (similar R² of 0.5 but decreased RMSE), due to the larger number of data points available for the curve fitting in larger grid sizes. Therefore, a grid resolution of 1°×1° was chosen in this study.

#### Validation of the recovery curves

The recovery curves were validated using field-based observations from Cook-Patton et al., (2020)<sup>2</sup>. We compared the field-based AGC and the AGC derived from the spatially-explicit regrowth curves following fire/other non-fire disturbances at the same grid in the corresponding age intervals. The comparison shows the spatially-explicit curves in general matched the site measurements across the three tropical continents (**Fig. 3-3c**). Our estimated AGC gain rate for the recovery forests at young stages (age < 20) with the previous studies based on remote sensing and site observations.

#### Calculation of the carbon gains and losses from post-disturbance recovery

The AGC loss from the disturbance is determined by the differences between the predisturbance AGC (**point a in Fig. 3-1**) and the remaining biomass (**point b**). The remaining biomass is calculated by multiplying the pre-disturbance AGC and the ratio of the biomass loss. The ratio of the biomass loss was determined using AGC<sub>max</sub> and intercept (d) from the corresponding recovery curve as below.

ratio= 
$$(AGC_{max}-d)/AGC_{max}$$
 (2)

For a forest pixel that has been disturbed before, pre-disturbance AGC is determined from the recovery curves by the period between the previous and the current disturbance events. For a forest pixel that has not been disturbed before (i.e., the first disturbance in the time series), we assumed that the biomass should be consistent with the surrounding undisturbed forest. The average AGC of N surrounding undisturbed forest pixels (N=10) was used to estimate the predisturbance AGC (point a) of the disturbed pixel.

For each disturbance event followed by forest recovery, the forest biomass gain depends on the differences between the current AGC (**point c in** Fig. 3-1) and the remaining AGC (**point b**). The current biomass was derived from the recovery curves at the corresponding grid and the period between the two disturbance events. The recovery curves for fire and other non-fire disturbances were applied for each corresponding disturbance event.

#### 3.1.4 Estimation of AGC changes for the undisturbed forest

esa	Ref	CCI Biomass Climate Assessment Report v3	
	Issue	Page	Date
	3.0	34	14.07.2021



To assess carbon dynamics in undisturbed forests, we first delineated the undisturbed forest extent in 2020 by excluding all pixels with recorded disturbance events from the forest extent. Forest extent was defined using a combination of regional land use/land cover products and global tree cover datasets (**Table 3-2**). AGC values for the undisturbed forest pixels were extracted from the CCI Biomass dataset. Using the biomass recovery curves fitted for each corresponding  $1^{\circ} \times 1^{\circ}$  grid cell, forest age in 2020 was estimated (backcasted) for each 30-meter pixel by identifying the time since the curve would have accumulated the observed AGC. Subsequently, AGC accumulation over the period 1985–2020 was estimated for each undisturbed forest pixel by combining the inferred forest age with the recovery trajectory:

$$C Gain_{undist} = AGC_{t=2020} - AGC_{t=1985}$$
(3)

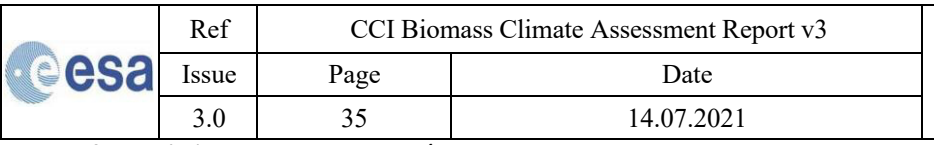
This approach assumes that these forests were free of detected disturbances in the Landsat record (post-1985), but may have experienced disturbances prior to 1985. It further assumes that post-disturbance recovery in these forests follows the same trajectory as recently disturbed forests, thereby enabling estimation of long-term C gains during 1985-2020.

Table 3-2 Forest extent data sources used in the analysis

Region	Forest class	Data source	Reference
	Coniferous		
Canada	Broad Leaf Mixedwood	Annual forest land cover maps for Canada's forested ecosystems	(Hermosilla et al. 2018) <sup>27</sup>
		European Forest	
Europe	Forest mask	Disturbance Atlas (EFDA)	Viana-Soto and Senf (2025) 18
US	Forest	Landscape Change monitoring System (LCCMS) (Land cover layer)	USDA Forest Service (2025)
China	Forest	China land cover dataset (CLCD)	Yang and Huang 2021 <sup>28</sup>
Tropics	Humid: Undisturbed forests/regrowth/degraded forests in 2020	Tropical Moist Forest (TMF) Tree cover and tree cover loss	Vancutsem et al. 2021 <sup>22</sup>
Порісз	Dry: tree cover in 2020 >25%	from Global Forest Watch (GFW)	(Hansen et al. 2013) <sup>29</sup>
Australia	Forest	National Forest and Sparse Woody Vegetation Data	Department of Climate Change, Energy, the Environment and Water (2023)
Other			
boreal/ Other	Tree cover >25% in 2020 from GFW	Tree cover and tree cover loss from Global Forest Watch (GFW)	(Hansen et al. 2013) <sup>29</sup>

#### 3.1.5 Estimation of AGC fluxes and turnover times

AGC fluxes at each  $1^{\circ} \times 1^{\circ}$  grid cell were defined as the mean annual gross AGC losses (resulting from disturbances and calculated following the procedures described in Method 3) divided by the total AGC stock in forests (eq. 4).





AGC fluxes (%)= AGC annual gross loss/Forest  $\overline{AGC_{stock}}$  x100

(4)

This metric quantifies the rate at which carbon is being released from (or cycling through) the forest ecosystem due to disturbances, relative to its standing biomass stock.

In contrast, AGC turnover time was calculated as the inverse relationship

Turnover time 
$$(yr)$$
=Forest  $AGC_{stock}$  /  $AGC_{annual\ gross\ loss}$  (5)

This value reflects the average time required for the existing AGC stock to be fully turned over under prevailing disturbance rates. As expected, regions with higher AGC fluxes tend to exhibit shorter turnover times, while lower fluxes correspond to more stable, longer-lived carbon stocks.

Total AGC stocks were estimated by summing aboveground biomass from the CCI-Biomass dataset across forested areas, as defined by a combination of regional and global forest land cover products (see Table 2).

#### 3.2 Global disturbed forest distribution and young forest age distribution

Globally, forests free of recorded disturbances from existing disturbance datasets since 1985 dominate the total forest area (accounting for 70%, 2330 Mha of the total forest area), while disturbed forests affected by events such as fire and harvest between 1985 and 2020 make up the remaining 30% in 2020 (Fig. 3-2). In recent years, there has been a notable increase in the extent of young forest stands, particularly in regions such as the tropics, Europe, and the United States (Fig. 3-2b). This increasing proportion of younger forest stands indicates more frequent and widespread disturbance events recently, probably driven by logging, fire and other pressures leading to degradation, resulting in accelerated forest regeneration and a higher prevalence of younger forest stands.

Regionally, tropical and sub-tropical regions are characterized by relatively higher rates of disturbances and younger forest age structures, while temperate and boreal zones maintain reservoirs of older and undisturbed stands (Fig. 3-2). Among all regions, Australia shows the largest area of disturbed forests in 2020, with only 26% of its forests remaining undisturbed. Following Australia, the dry tropics have the second largest proportion of disturbed forests (55%) and show the highest proportion of youngest forests aged from 1–10 years (41%). due to the frequent repeated fire and rapid regeneration cycles across this region 28,29. In humid tropical regions, the forest age among disturbed forests is more evenly distributed, with 10% aged 0–10 years and 13% aged 10–30 years, respectively. Temperate and boreal regions, including China (84%), Canada (76%), the United States (76%), and Europe (76%), are dominated by undisturbed forests. These regions maintain older forest structures with limited recent disturbance, acting as important reservoirs of long-standing biomass and carbon storage.

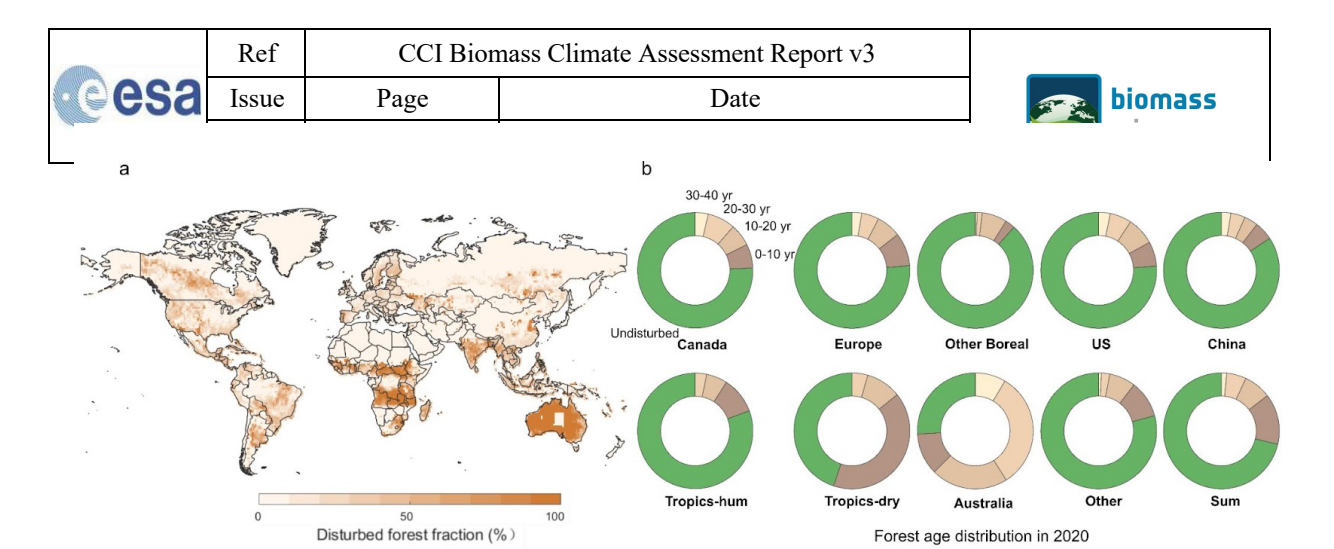


Figure 3-2 Global distribution of disturbed forests and forest age structure in 2020. a) Fraction of forest area disturbed during 1985-2020 within each 1° grid cell. b) Forest age composition in 2020, with each donut chart showing the proportion of young forests that regenerated following disturbances during 1985–2020 and ageing forests that remained undisturbed over the same period. Young forests are classified into four age groups (0–10, 11–20, 21–30, and 31–40 years) based on the time since the last disturbance, derived from regional disturbance datasets. Regional boundaries correspond to those shown in Fig. 2c.

#### 3.3 Forest regrowth patterns across global regions

By utilizing satellite-derived disturbance history maps and the CCI Biomass dataset, we derived regional forest regrowth curves by fitting a Richard-Chapman model to aboveground carbon (AGC) values as a function of forest age since the last disturbance, using a space-for-time substitution approach. This method captures the trajectory of biomass recovery after disturbance at a 1° grid resolution across the global forest area.

The shape and pace of regrowth vary markedly across regions. In the tropics, AGC accumulation is rapid, reaching close to saturation within the first 30–40 years since the disturbance, indicating high productivity and fast biomass recovery in tropical forest systems. In contrast, temperate and boreal regions such as Canada, the US, Europe, and other boreal regions exhibit much slower AGC recovery, with more gradual increases in biomass over time. The median AGC gain rates between 0-30 years are particularly high in the tropics (> 4 MgC ha<sup>-1</sup> yr<sup>-1</sup>, followed by moderate rates in China and the US (~2–3 MgC ha<sup>-1</sup> yr<sup>-1</sup>). Boreal and temperate regions such as Canada and Europe show slower growth, with estimated rates of ~1–2 MgC ha<sup>-1</sup> yr<sup>-1</sup>.

To validate our regrowth estimates, we compared AGC accumulation rates during the first 30 years post-disturbance with independent values from Cook-Patton et al. (2020)<sup>2</sup>. Overall, our modeled results show good agreement with Cook-Patton data, particularly in boreal regions where estimates closely align. In temperate and tropical regions, our models tend to reflect slightly more region-specific variability and lower AGC gain rates, but remain within the expected range of early regrowth dynamics (Fig. 3-3b).

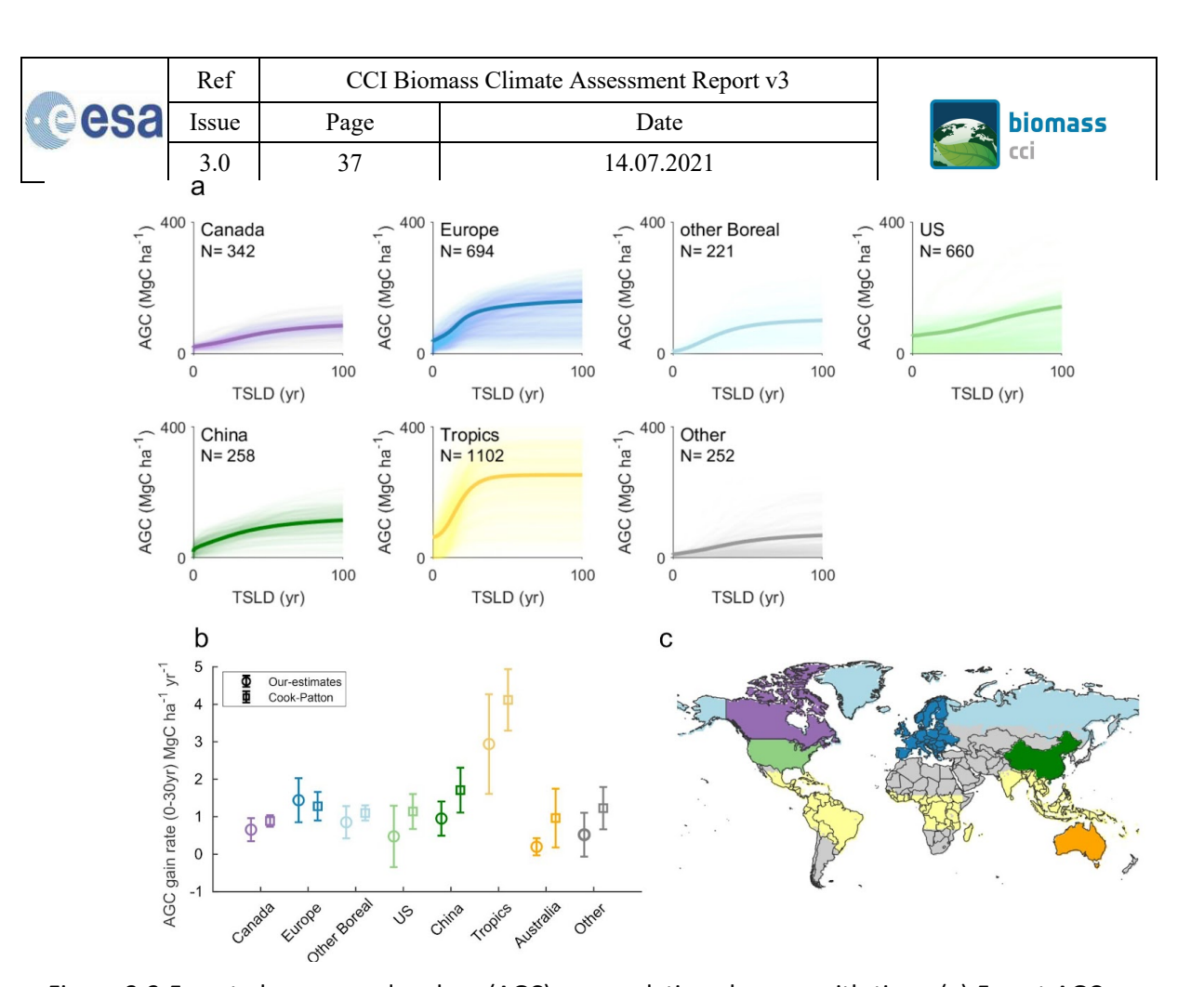


Figure 3-3 Forest aboveground carbon (AGC) accumulation changes with time. (a) Forest AGC accumulation as a function of forest age for each study region. (b) Comparison of AGC accumulation rates over first 0-100 years after regrowth with estimates from naturally regenerating forests reported by Cook-Patton et al.  $(2020)^2$ . (c) Regional map used in the analysis. Each color-coded region corresponds to those used in panels a and b. AGC growth curves at 1° grid cell were fitted using the Richards-Chapman function (AGC = AGC<sub>max</sub> × (1 – exp(–bt))<sup>c</sup>)+d based on the time since the last disturbance (t) derived from the regional disturbance histories and the 2020 forest biomass map (see Methods).

### 3.4 Spatial and temporal dynamics of forest AGC change associated with disturbances

By combining regional disturbance histories with the modeled regrowth curves, we assessed the spatial and temporal dynamics of forest AGC changes associated with disturbances from 1985 to 2020. At the global scale, forests disturbed during this period gained +18.9 PgC through post-disturbance recovery but lost -27.3 PgC due to fire and non-fire disturbances, resulting in a net AGC loss of -8.5 PgC since 1985.

The tropics contributed the largest to the global net AGC losses, accounting for 83% (–7.1 PgC) of the global net losses (Fig. 3-4). Among which, dry tropical forests experienced the highest gross AGC losses, primarily driven by fire disturbances (–12.1 PgC). However, due to relatively rapid post-fire recovery (Fig. 3-3) in these fire-adapted ecosystems, +10.8 PgC of AGC was regained, offsetting a substantial portion (90%) of the fire-driven losses and resulting in a near-neutral carbon balance. In contrast, the humid tropics showed the largest net AGC loss globally (–5.8 Pg C), primarily due to non-fire disturbances such as logging and degradation. Gross AGC

esa	Ref	CCI Biomass Climate Assessment Report v3	
	Issue	Page	Date
	3.0	38	14.07.2021



losses and gains were concentrated in well-known tropical hotspots, including the "Arc of Deforestation" in the Amazon, Northern and Southern Central Africa, and Southeast Asia, where both fire and degradation pressures are extensive. Note that land use change-related C fluxes (e.g., deforestation and afforestation) were excluded from this analysis due to inconsistencies between regional and global land cover datasets (e.g., ESA-CCI LC product, Global Forest Watch, and regional land cover products).

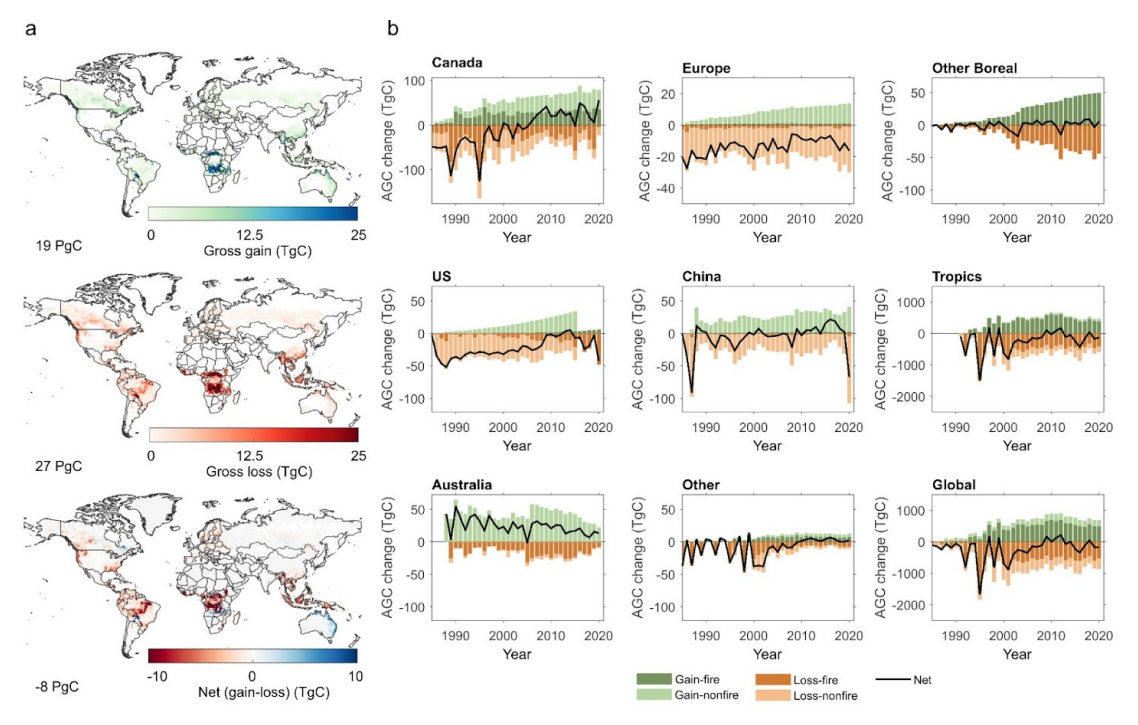
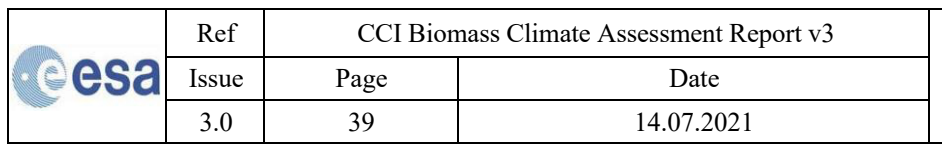


Figure 3-4 Spatial and temporal dynamics of forest AGC change associated with disturbances during 1985–2020. (a) Spatial patterns of gross AGC gains, gross AGC losses, and net AGC changes. (b) Temporal dynamics of AGC change by study region. Bars show annual carbon losses and gains due to fire and non-fire disturbances. Black lines indicate the annual net AGC balance, calculated as the sum of all carbon flux components. Data availability varies by region based on the coverage of regional disturbance datasets: for example, the United States (1990–2015), the Tropics (1990–2020), and Australia (1988–2020). In regions lacking regional datasets (i.e., Other Boreal and Other regions), a global burned area dataset was used <sup>21</sup>. Note that fire data has an ~8-year gap in the early record (post-1985) due to limited Landsat availability.

Outside the tropics, Australia was the only region to exhibit a net AGC gain (+0.7 Pg C), largely driven by regrowth following past woody vegetation and non-vegetated area. However, this AGC gain has declined in recent decades due to increasing fire activity (**Fig. 3-4**). In contrast, temperate and boreal regions such as the US, Europe, and China experienced moderate net AGC losses, from -0.01 to -0.8 Pg C, primarily due to non-fire disturbances such as wood harvesting. Canada presents a different disturbance pattern, with both fire and non-fire disturbance shaping AGC dynamics. While some fluctuations occurred in recent years (e.g., in Europe and China), these regions generally showed increasing AGC gains since 1985, unlike Australia.

It is important to note that limitations in long-term disturbance data, such as the lack of consistent differentiation between fire and non-fire disturbances, constrain detailed pan-boreal assessments, particularly for Russian boreal forests.





#### 3.5 Forest regrowth patterns across global regions

We further examined the spatial and regional variability in AGC stock and turnover characteristics using forest disturbance, biomass, and forest extent data for the period 2001–2020. The global forest ecosystems exhibited an annual AGC turnover (i.e., gross AGC losses) of 0.77 Pg C yr<sup>-1</sup>, corresponding to a global average turnover rate of 0.38% yr<sup>-1</sup> and a turnover time of 262 years. However, these AGC turnover and turnover characteristics show strong spatial and regional variability (Fig. 3-5). The highest turnover rates were observed in fire-prone and intensively managed forests, particularly in tropical and temperate regions, while boreal forests in general exhibited the longest turnover times due to slower growth and recovery.

The tropics store the largest share of AGC stock globally, contributing 74% (0.57 Pg C yr $^{-1}$ ) of the global annual AGC turnover (74%, 0.57 Pg C yr $^{-1}$ ). Despite a moderate turnover rate of 0.41% yr $^{-1}$  among the global regions, the vast forest extent, high carbon storage, and frequent disturbances from both human and natural drivers result in the highest global AGC turnover fluxes in this biome. The average turnover time in tropical forests is 245 years, indicating a dynamic balance between disturbance and relatively rapid biomass accumulation.

In Australia, forests showed the highest turnover rate (1.17%) and the shortest turnover time (85 years), primarily driven by fires, which account for 84% of the annual AGC turnover in this region.

Among boreal and temperate regions, Canada exhibits a relatively high AGC turnover rate (0.80% yr<sup>-1</sup>) and faster AGC turnover time (126 years). The United States and China exhibit moderate turnover rates of 0.34% yr<sup>-1</sup> and 0.44% yr<sup>-1</sup>, with corresponding turnover times of 296 years and 229 years, respectively, driven largely by non-fire activities such as logging. In contrast, Europe shows a lower average turnover rate (0.20% yr<sup>-1</sup>) and a longer turnover time (505 years). Across Europe, these values vary substantially, with higher turnover rates observed in intensively managed boreal forests and lower rates in temperate continental zones. The remaining boreal forests, including those in Russia and Alaska, show the lowest turnover rate (0.09%) and the longest turnover time (1101 years), indicating extremely slow carbon cycling and limited post-disturbance recovery in these low-productivity ecosystems. Note that the turnover time may be underestimated in regions with incomplete disturbance data, particularly in the Russian boreal zone.

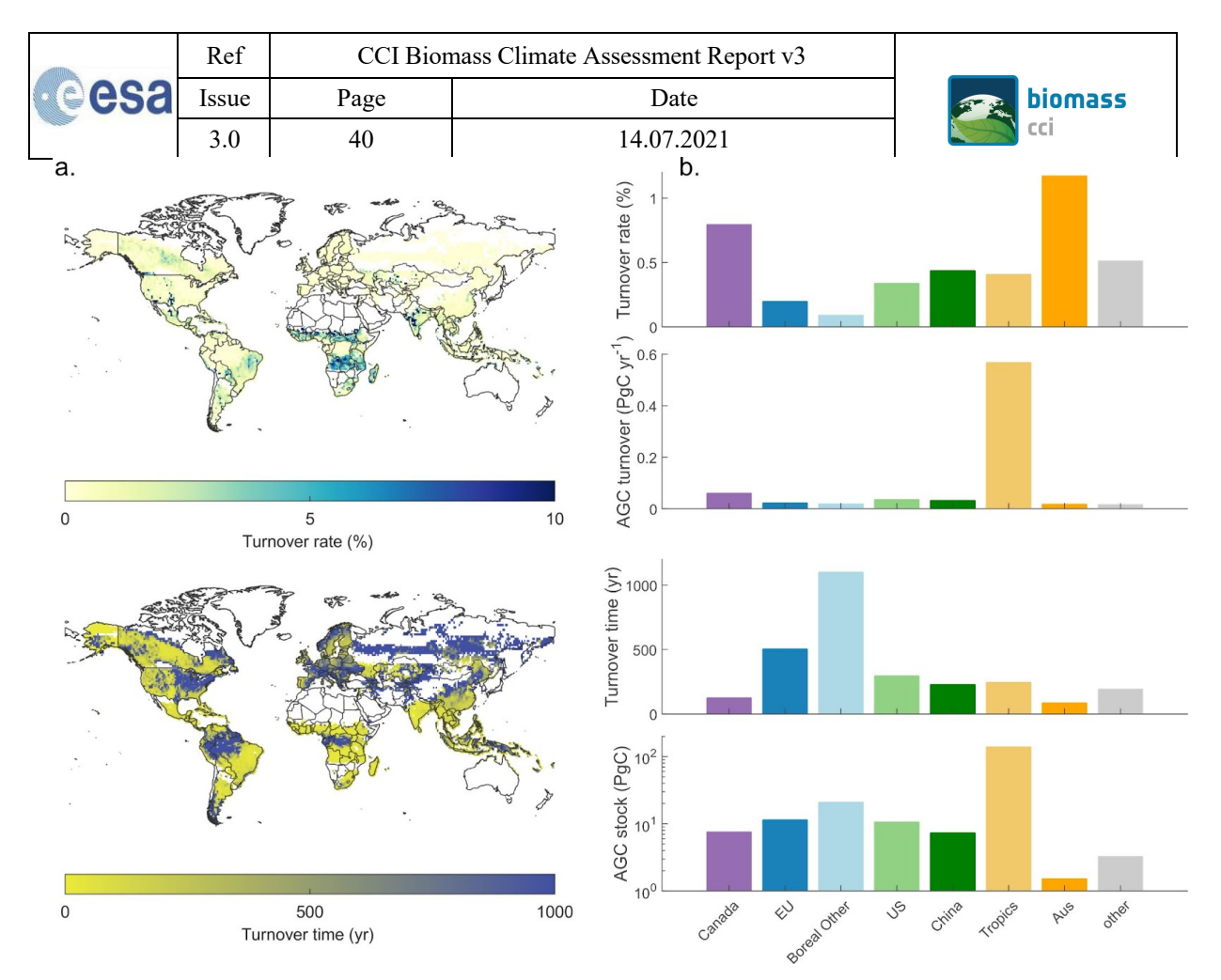


Figure 3-5 Global and regional distributions of forest AGC fluxes and turnover times. (a) Spatial distribution of AGC fluxes, calculated as the ratio of gross AGC losses to total AGC stock at each 1° grid cell. (c) Spatial distribution of AGC turnover time, defined as the ratio of total AGC stock to gross AGC losses from disturbances during 1985–2020. (b) Regional averages of AGC turnover rate and AGC turnover (PgC yr<sup>1</sup>), (d) Regional averages of turnover times/AGC stock (d), corresponding to the maps in a and b.

#### 3.6 Reference

- 1. Pugh, T. A. M., Arneth, A., Kautz, M., Poulter, B. & Smith, B. Important role of forest disturbances in the global biomass turnover and carbon sinks. Nat Geosci 12, 730–735 (2019).
- 2. Cook-Patton, S. C. et al. Mapping carbon accumulation potential from global natural forest regrowth. Nature 585, 545–550 (2020).
- 3. Seidl, R. et al. Forest disturbances under climate change. Nat Clim Chang 7, 395–402 (2017).
- 4. Neigh, C. S. R. et al. Russian forests show strong potential for young forest growth. Commun Earth Environ 6, 71 (2025).
- 5. Maltman, J. C., Hermosilla, T., Wulder, M. A., Coops, N. C. & White, J. C. Estimating and mapping forest age across Canada's forested ecosystems. Remote Sens. Environ. 290, 113529 (2023).
- 6. Bousfield, C. G. & Edwards, D. P. The pan-tropical age distribution of regenerating tropical moist forest. Nat Ecol Evol (2025) doi:10.1038/s41559-025-02721-8.
- 7. Besnard, S. et al. Global covariation of forest age transitions with the net carbon balance. Research Square (2024) doi:10.21203/rs.3.rs-4655317/v1.
- 8. Besnard, S. et al. Mapping global forest age from forest inventories, biomass and climate data. Earth Syst. Sci. Data 13, 4881–4896 (2021).

esa	Ref	CCI Bion	nass Climate Assessment Report v3	
	Issue	Page	Date	
	3.0	41	14.07.2021	



- 9. Neigh, C. S. R. et al. Russian forests show strong potential for young forest growth. Commun Earth Environ 6, 71 (2025).
- 10. Houghton, R. A. & Castanho, A. Annual emissions of carbon from land use, land-use change, and forestry from 1850 to 2020. Earth Syst. Sci. Data 15, 2025–2054 (2023).
- 11. Hansis, E., Davis, S. J. & Pongratz, J. Relevance of methodological choices for accounting of land use change carbon fluxes. Global Biogeochemical Cycles 29, 1230–1246 (2015).
- 12. Gasser, T. & Ciais, P. A theoretical framework for the net land-to-atmosphere CO2 flux and its implications in the definition of 'emissions from land-use change'. Earth Syst. Dyn. 4, 171–186 (2013).
- 13. Dye, A. W. et al. Carbon, climate, and natural disturbance: a review of mechanisms, challenges, and tools for understanding forest carbon stability in an uncertain future. Carbon Balance Manag 19, 35 (2024).
- 14. O'Sullivan, M. et al. The key role of forest disturbance in reconciling estimates of the northern carbon sink. Commun. Earth Environ. 5, (2024).
- 15. Grassi, G. et al. Harmonising the land-use flux estimates of global models and national inventories for 2000–2020. Earth Syst. Sci. Data 15, 1093–1114 (2023).
- 16. Hermosilla, T., Wulder, M. A., White, J. C. & Coops, N. C. Prevalence of multiple forest disturbances and impact on vegetation regrowth from interannual Landsat time series (1985–2015). Remote Sens. Environ. 233, 111403 (2019).
- 17. Hermosilla, T. et al. Mass data processing of time series Landsat imagery: pixels to data products for forest monitoring. International Journal of Digital Earth 1035–1054 (2016).
- 18. Viana-Soto, A. & Senf, C. The European Forest Disturbance Atlas: a forest disturbance monitoring system using the Landsat archive. Earth System Science Data 17, 2373–2404 (2025).
- 19. Lu, J., Huang, C., Tao, X. & Schleeweis, K. NACP NAFD project: Forest disturbance intensity for CONUS from Landsat, 1986-2015. Preprint at https://doi.org/10.3334/ORNLDAAC/2059 (2023).
- 20. Liu, Z. et al. Forest disturbance decreased in China from 1986 to 2020 despite regional variations. Commun. Earth Environ. 4, (2023).
- 21. Long, T. et al. 30 m resolution global annual Burned Area mapping based on Landsat images and Google Earth Engine. Remote Sens. (Basel) 11, 489 (2019).
- 22. Vancutsem, C. et al. Long-term (1990-2019) monitoring of forest cover changes in the humid tropics. Sci Adv 7, (2021).
- 23. United States Geological Survey, US Forest Service & Nelson, K. Monitoring Trends in Burn Severity (ver. 12.0, April 2025). U.S. Geological Survey https://doi.org/10.5066/P9IED7RZ (2021).
- 24. Estimation of boreal forest biomass from ICESat-2 data using hierarchical hybrid inference. Remote Sensing of Environment 311, 114249 (2024).
- 25. Liu, S. et al. The overlooked contribution of trees outside forests to tree cover and woody biomass across Europe. Science Advances (2023) doi:10.1126/sciadv.adh4097.
- 26. Potapov, P. et al. The last frontiers of wilderness: Tracking loss of intact forest landscapes from 2000 to 2013. Sci Adv 3, e1600821 (2017).
- 27. Hermosilla, T., Wulder, M. A., White, J. C., Coops, N. C. & Hobart, G. W. Disturbance-informed annual land cover classification maps of Canada's forested ecosystems for a 29-year Landsat time series. Can. J. Remote Sens./J. Can. Teledetect. 44, 67–87 (2018).
- 28. Yang, J. & Huang, X. The 30 m annual land cover dataset and its dynamics in China from 1990 to 2019. Earth Syst. Sci. Data 13, 3907–3925 (2021).
- 29. Hansen, M. C. et al. High-resolution global maps of 21st-century forest cover change. Science 342, 850–853 (2013).
- 30. Bousfield, C. G. & Edwards, D. P. The pan-tropical age distribution of regenerating tropical moist forest. Nat Ecol Evol (2025) doi:10.1038/s41559-025-02721-8.
- 31. Silvestrini, R. A. et al. Simulating fire regimes in the Amazon in response to climate change and deforestation. Ecol Appl 21, 1573–1590 (2011).
- 32. Saito, M. et al. Fire regimes and variability in aboveground woody biomass in miombo woodland. J. Geophys. Res. Biogeosci. 119, 1014–1029 (2014).
- 33. Besnard, S., Heinrich, V., Carvalhais, N., Ciais, P., Herold, M., Luijkx, I., ... & Yang, H. (2024). Global covariation of forest age transitions with the net carbon balance.